Composites: Part B 69 (2015) 317–334

Contents lists available at ScienceDirect

Composites: Part B

journal homepage: www.elsevier.com/locate/compositesb

Thermoelastic analysis of advanced sandwich plates based on a new quasi-3D hybrid type HSDT with 5 unknowns

J.L. Mantari [a,*], E.V. Granados [b]

[a] Faculty of Mechanical Engineering, University of Engineering and Technology, Av. Cascanueces 2281, Santa Anita, Lima, Peru
[b] Faculty of Mechanical Engineering, National University of Engineering, Av. Túpac Amaru 210, Rimac, Lima, Peru

ARTICLE INFO

Article history:
Received 28 August 2014
Received in revised form 29 September 2014
Accepted 1 October 2014
Available online 13 October 2014

Keywords:
A. Layered structures
A. Plates
B. Elasticity
B. Thermomechanical
C. Analytical modeling

ABSTRACT

This paper presents a thermoelastic bending analysis of functionally graded sandwich plates by using a new quasi-3D hybrid type higher order shear deformation theory (HSDT). The mathematical model contains only 5 unknowns as the first order shear deformation theory (FSDT). The nonlinear term of the temperature field is modeled in such way that can be different from the shape functions of the displacement field. The mechanical properties of functionally graded layers of the plate are assumed to vary in the thickness direction according to a power law distribution. The governing equations for the thermoelastic bending analysis are obtained through the principle of virtual work and solved via Navier-type solution. Results reveal: (a) the good performance of the present generalized formulation; (b) the significant influence of the nonlinear temperature field on the displacements and stresses results. Consequently, discussion on nonlinear temperature field influences should be further considered in the literature.

1. Introduction

Composite materials are alternative materials utilized extensively in construction or fabrication of structures due to the high performance and reliability [1]. Mainly, there are two types of constructions with composite materials; the single skin and the sandwich construction [2,3]. The sandwich construction is noted for its exceptional stiffness-to-weight ratio compared with other structures. Classical sandwich construction is often used in ship structures because of its main features; such as high flexural resistance, high impact strength (carbon fibers), high corrosion resistance (glass fibers) and the low thermal and acoustics conductivity [4,5]. In the last decades the use of sandwich construction grew rapidly around the world. Its advantages, the development of new materials and the necessity of high performance under static, dynamic and thermal loads guarantee that the sandwich structures will be in demand for many years [6–8]. With the increased use of sandwich structures, there is a tremendous need to develop efficient manufacturing techniques, economical and effective repair techniques, and analysis methods to predict the short and long-term behavior of the multilayer composite materials under a variety of loading and environmental conditions.

Normally, a sandwich plate is composed of skins (inner and outer layers) and the core. The core of the sandwich plate is a very important component in layered structures. Several types of cores have been developed for different applications; among them are the honeycomb, foam, web, and solid type such as a functionally graded (FG) core. In recent years the behavior of sandwich structures made of functionally graded materials (FGMs) are being studied. FGMs are produced for example by mixing two or more materials in a certain volume ratio. The continuous nature of the variation of the material properties in FGMs lessens both thermal and residual stresses. Thus, the known advantages of FGMs are incorporated in the sandwich construction for several engineering applications. A sandwich construction can be composed of a FG core and two homogeneous skins or a homogeneous core and two FG skins.

A literature review reveals that many theories have been developed to study the behavior of structures composed of layers. These theories can be classified in different models, such as equivalent single layer (ESL), quasi-layerwise and layerwise models. HSDTs were developed to improve the analysis of plate responses and extensively used by many researchers. Normally, these theories comply with the free surface boundary conditions and account for approximately parabolic distribution of shear stresses through the thickness of the plate. On the other hand, layerwise theories may provide a better representation of interlaminar stresses (continuous transverse stresses at layer interfaces) and moderate

* Corresponding author. Tel.: +51 13540070, cell: +51 96224551.
E-mail address: jmantari@utec.edu.pe (J.L. Mantari).

http://dx.doi.org/10.1016/j.compositesb.2014.10.009
1359-8368/

to severe cross-sectional warping, thus they allow to analyze the local behavior of laminated structures when needed (e.g. modeling damage, impact, non-linear effects), but they may be computationally too expensive.

In general, the structures are subjected to mechanical load and temperature changes both internally and externally. Then, it is important to analyze the behavior of structural elements subjected to mechanical or thermal loads or a combination of both. In this sense, many authors investigated the thermo-mechanical behavior of sandwich plates by using HSDTs with both layerwise and ESL approaches.

Polit and Touratier [9] presented a new six-node multilayered triangular finite element based on a HSDT to analyze the behavior of sandwich plates under mechanical load. The theory takes into account the interlaminar continuity of the transverse shear stresses. Kant and Swaminathan [10] presented an analytical solution for the static analysis of sandwich plates subjected to mechanical load based on a quasi-3D HSDT with 12 unknowns. Matsunaga [11] expanded the displacement components with power series for the analysis of sandwich plates under thermal loads by using a 2D HSDT. Ferreira et al. [12] presented the static analysis of sandwich plates under mechanical loads by using multiquadric discretization and a FSDT layerwise theory. Zenkour and Alghamdi [13] analyzed the response of FG sandwich plates subjected to thermal load based on quasi-3D HSDT. The authors considered that the function of the nonlinear term of the temperature field is equal to the shape function of the displacement field. Xiang et al. [14] studied the static behavior of sandwich plates under mechanical loads by discretizing several HSDTs by a meshless method based on inverse multiquadric radial basis functions. Cetkovic and Vuksanovic [15] used a generalized layerwise theory to study the sandwich plates under mechanical loads. This theory assumes transverse variation of the in-plane displacement components in terms of 1D linear Lagrangian finite elements. Shariyat [16,17] presented a linear and nonlinear bending analysis of sandwich plate under thermomechanical loads based on generalized 3D high-order double superposition global–local theory, respectively. Zenkour [18] analyzed the thermal buckling of FG sandwich plates subjected to uniform temperature rise or a graded temperature change across the thickness. The author utilized a sinusoidal shear deformation plate theory (SSDT) and the non-linear von Karman strain–displacement equations. Mantari et al. [19–21] analyzed the behavior of a sandwich plate subjected to mechanical loads based on news HSDTs. The ESL shear deformation theory developed in [20] was extended to layerwise shear deformation theory for the finite element analysis of sandwich plates under mechanical loads in [22]. Natarajan and Manickam [23] employed a C^0 8-noded quadrilateral plate element with 13 degrees of freedom per node based on a HSDT to study the static behavior of FG sandwich plates. Nguyen et al. [24] presented a formulation based on isogeometric finite element approach associated with a HSDT to study the static and buckling behavior of sandwich plate under mechanical loads. Thai et al. [25] also presented the static and buckling analysis of sandwich plate under mechanical loads based on isogeometric layerwise finite element approach. Grover et al. [26] developed a new inverse hyperbolic shear deformation theory for the bending and buckling analysis of sandwich plates considering a displacement field with 5 unknowns without thickness stretching effect. Neves et al. [27] presented the static and buckling analysis of FG sandwich plates under mechanical loads based on a HSDT with thickness stretching effect. The authors utilized the Carrera's Unified Formulation (CUF) to obtain the governing equations, then, the static and eigenvalue problems were solved by collocation with radial basis functions. Further extension of CUF can be seen in Refs. [28–33].

Recently, Golmakani [34] studied the large deflection analysis of FG solid and hollow rotating axisymmetric disk with uniform and variable thickness subjected to thermo-mechanical loading. Torabi et al. [35] investigated the buckling analysis of a FG conical shell integrated with piezoelectric layers that is subjected to combined action of thermal and electrical loads. Malekzadeh and Monajjemzadeh [36] studied the dynamic response of FGPs in thermal environment under a moving load and elastic foundation. The equations are derived based on the FSDT including the effects of initial thermal stresses induced by the thermal environment. Kiani and Eslami [37] presented an exact solution for thermal buckling of annular FGM plates on an elastic medium. Hamidi et al. [38] developed a refined 2D shear deformation theory with four unknowns for the bending analysis of FG sandwich plates under thermomechanical loads considering a nonlinear temperature field with a polynomial function. Houari et al. [39] analyzed the sandwich plates with functionally graded skins under thermal load by using a HSDT with thickness stretching effect. Tounsi et al. [40] presented the bending analysis of sandwich plates with functionally graded core based on refined shear deformation theory. The last two papers considered a temperature field with a sine function in the nonlinear term.

This paper presents an analytical solution of the thermoelastic bending problem of FG sandwich plates by using a new quasi-3D hybrid type HSDT. The displacement field contains two shear strain shape functions, i.e. $f(z)$ and $g(z)$. Normally non-polynomial shear strain shape functions, such as trigonometric, trigonometric hyperbolic, exponential, etc., can be used in classical HSDTs and in general $g(z) = f'(z)$. Therefore, in most of the formulation presented in the literature, it is not free to choose the shear strain shape function $g(z)$. The present generalized formulation has that freedom, and infinite hybrid type shear deformation theories (polynomial or non-polynomial or hybrid type) can be created just having five unknowns, i.e. if desired $g(z)$ can be different from $f'(z)$. This generalized quasi-3D hybrid type HSDT accounts for adequate distribution of the transverse shear stresses through the plate thickness and tangential stress-free boundary conditions on the plate boundary surface, thus a shear correction factor is not required. The nonlinear term of the temperature field can be different from the shape functions of the displacement field. The mechanical properties of functionally graded layers of the plate are assumed to vary in the thickness direction according to a power law distribution in terms of the volume fractions of the constituents. The governing equations for the thermoelastic bending analysis are obtained through the principle of virtual works. These equations are then solved via Navier solution. The solutions are obtained for simply supported sandwich plates subjected to a transverse thermal bi-sinusoidal load. The performance of the theory is verified by comparing results with other quasi-3D HSDTs and 2D HSDTs available in literature.

2. Analytical modeling

The mathematical model was built to solve two types of FG sandwich plates. The sandwich plates of uniform thickness "h", length "a", and width "b" are shown in Figs. 1 and 2. The rectangular Cartesian coordinate system x, y, z, has the plane $z = 0$, coinciding with the mid-surface of the plates. The vertical positions of bottom, the two interfaces and the top surface of the sandwich plate are denoted by $h_1 = -h/2$, h_2, h_3, $h_4 = h/2$, respectively. The ratio of the thickness of each layers from bottom to top is denoted by the combination of three numbers, for example, a symmetric sandwich plate composed of three layers of equal thickness will have a configuration or scheme "1-1-1" ($h_2 = -h/6$, $h_3 = h/6$).

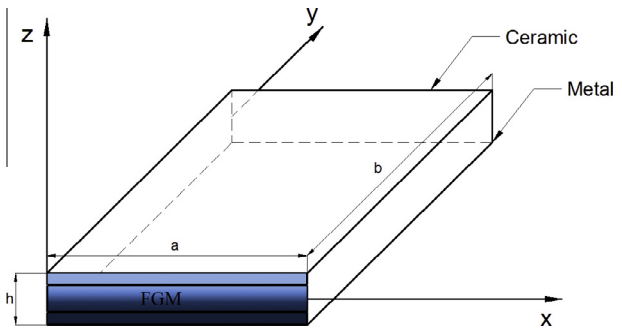

Fig. 1. Geometry of functionally graded sandwich plate A-type.

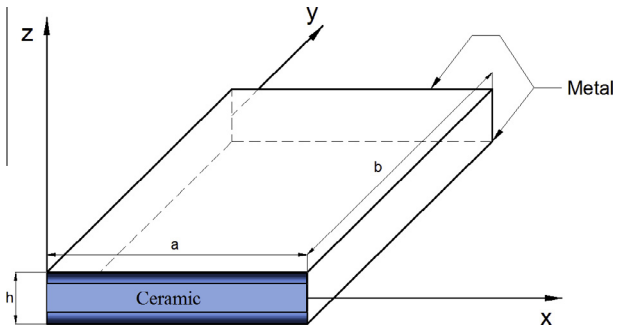

Fig. 2. Geometry of functionally graded sandwich plate B-type.

2.1. Functionally graded sandwich plates

The material properties for the functionally graded layers vary through the thickness with a power law distribution, which is given below:

$$P^{(k)}_{(z)} = (P^{(k)}_t - P^{(k)}_b)V^{(k)}_{(z)} + P^{(k)}_b \tag{1}$$

where $P^{(k)}$ denotes the effective material property, $P^{(k)}_t$ and $P^{(k)}_b$ denote the property of the top and bottom faces of the functionally graded layer, respectively, and "k" represent a single-layer of the sandwich plate, i.e., $k = 1, 2, 3$ for the bottom, middle and top layer, respectively. The effective material properties of the plate, including Young's modulus, E, and shear modulus, G, and the thermal expansion coefficients, "α", vary according to Eq. (1). Generally, Poisson's ratio, "ν", varies in a small range. For simplicity, "ν" is assumed constant.

The sandwich plate A-type is composed of three layers, a functionally graded core and two isotropic skins as shown in Fig. 1. The bottom skin is rich in metal and the top skin is rich in ceramic. Therefore, the volume fraction for the ceramic phase $V^{(k)}$ (see Eq. (1)) is expressed as (see Fig. 3):

$$\begin{aligned} V^{(1)}_{(z)} &= 0, \quad h_1 \leqslant z \leqslant h_2 \\ V^{(2)}_{(z)} &= \left(\frac{z-h_2}{h_3-h_2}\right)^p, \quad h_2 \leqslant z \leqslant h_3 \\ V^{(3)}_{(z)} &= 1, \quad h_3 \leqslant z \leqslant h_4 \end{aligned} \tag{2a-c}$$

where "p" is the exponent that specifies the material variation profile through the thickness ($0 \leqslant p \leqslant \infty$).

The sandwich plate B-type is composed of three layers, an isotropic core and two functionally graded skins as shown in Fig. 2. The core is a fully ceramic layer, the bottom layer is made of a mixture of materials from metal to ceramic and the top layer is made of a mixture of materials from ceramic to metal. For this case, the volume fraction for the ceramic phase $V^{(k)}$ is expressed as (see Fig. 4):

$$\begin{aligned} V^{(1)}_{(z)} &= \left(\frac{z-h_1}{h_2-h_1}\right)^p, \quad h_1 \leqslant z \leqslant h_2 \\ V^{(2)}_{(z)} &= 1, \quad h_2 \leqslant z \leqslant h_3 \\ V^{(3)}_{(z)} &= \left(\frac{z-h_4}{h_3-h_4}\right)^p, \quad h_3 \leqslant z \leqslant h_4 \end{aligned} \tag{3a-c}$$

From the above equations can be stated that if the exponent is equal to zero ($p = 0$), the layer acquires the material properties of the top surface. Likewise, if the exponent is equal to infinity ($p = \infty$), the layer acquires the material properties of the bottom surface. These considerations are important when studying a homogeneous material.

2.2. Displacement base field

The displacement field satisfying the conditions of transverse shear stresses (and hence strains) vanishing at a point $(x, y, \pm h/2)$ on the outer (top) and inner (bottom) surfaces of the plate, is given as follows (see [41]):

$$\begin{aligned} \bar{u} &= u + z\left[y^{**}\frac{\partial w_b}{\partial x} + q^*\frac{\partial \theta}{\partial x} - \frac{\partial w_s}{\partial x}\right] + f(z)\frac{\partial w_b}{\partial x} \\ \bar{v} &= v + z\left[y^{**}\frac{\partial w_b}{\partial y} + q^*\frac{\partial \theta}{\partial y} - \frac{\partial w_s}{\partial y}\right] + f(z)\frac{\partial w_b}{\partial y} \\ \bar{w} &= w_b + w_s + g(z)\theta \end{aligned} \tag{4a-c}$$

where $u(x,y)$, $v(x,y)$, $w_b(x,y)$, $w_s(x,y)$, $\theta(x,y)$ are the five unknown displacement functions of the middle surface of the panel, whilst $y^{**} = y^* - 1, y^* = -f'\left(\frac{h}{2}\right)$ and $q^* = -g\left(\frac{h}{2}\right)$. In Eq. (4a-c), the classical term w_0 is written as the sum of w_b and w_s to separate the term responsible for *bending* and that for *shear* (see the subscripts); and the in-plane higher order unknown terns are defined as a functions of w_b, i.e. $\frac{\partial w_b}{\partial x}$, $\frac{\partial w_b}{\partial y}$. In this paper the displacement field contains a shape functions expressed as:

$$f(z) = h\sinh\left(\frac{z}{h}\right)e^{-2\left(\frac{z}{h}\right)^2}, \quad g(z) = \cos\left(\frac{\pi z}{h}\right) \tag{5a, b}$$

2.3. Kinematic relations and constitutive relations

In the derivation of the necessary equations, small strains are assumed (i.e., displacements and rotations are small, and obey Hooke's law and the elasticity theory). The linear strain expressions derived from the displacement model of Eq. (4a-c), valid for thin, moderately thick and thick plate under consideration are as follows:

$$\begin{aligned} \varepsilon_{xx} &= \varepsilon^0_{xx} + z\varepsilon^1_{xx} + f(z)\varepsilon^2_{xx} \\ \varepsilon_{yy} &= \varepsilon^0_{yy} + z\varepsilon^1_{yy} + f(z)\varepsilon^2_{yy} \\ \varepsilon_{zz} &= g'(z)\varepsilon^5_{zz} \\ \varepsilon_{yz} &= \varepsilon^0_{yz} + g(z)\varepsilon^3_{yz} + f'(z)\varepsilon^4_{yz} \\ \varepsilon_{xz} &= \varepsilon^0_{xz} + g(z)\varepsilon^3_{xz} + f'(z)\varepsilon^4_{xz} \\ \varepsilon_{xy} &= \varepsilon^0_{xy} + z\varepsilon^1_{xy} + f(z)\varepsilon^2_{xy} \end{aligned} \tag{6a-f}$$

where

$$\begin{aligned} &\varepsilon^0_{xx} = \frac{\partial u}{\partial x}, \quad \varepsilon^1_{xx} = y^{**}\frac{\partial^2 w_b}{\partial x^2} + q^*\frac{\partial^2 \theta}{\partial x^2} - \frac{\partial^2 w_s}{\partial x^2}, \quad \varepsilon^2_{xx} = \frac{\partial^2 w_b}{\partial x^2} \\ &\varepsilon^0_{yy} = \frac{\partial v}{\partial y}, \quad \varepsilon^1_{yy} = y^{**}\frac{\partial^2 w_b}{\partial y^2} + q^*\frac{\partial^2 \theta}{\partial y^2} - \frac{\partial^2 w_s}{\partial y^2}, \quad \varepsilon^2_{yy} = \frac{\partial^2 w_b}{\partial y^2} \\ &\varepsilon^5_{zz} = \theta, \end{aligned}$$

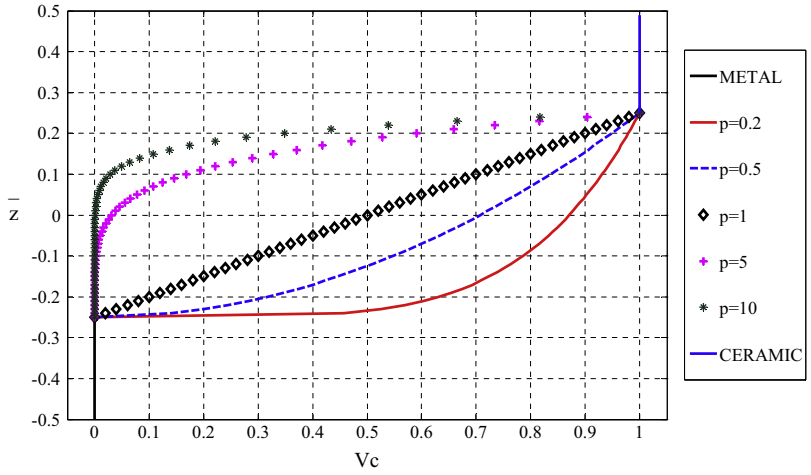

Fig. 3. Volume fraction for the ceramic phase, $V_{(z)}$, along the thickness of a functionally graded sandwich plate A-type for different values of the exponent "p" (1-2-1).

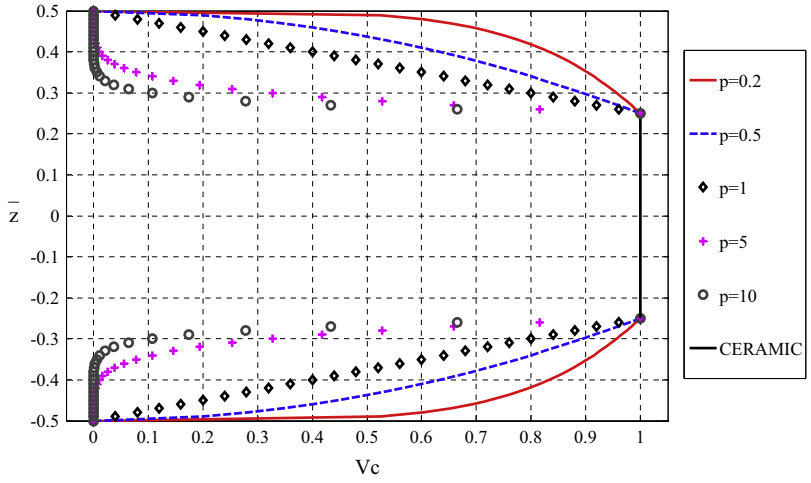

Fig. 4. Volume fraction for the ceramic phase, $V_{(z)}$, along the thickness of a functionally graded sandwich plate B-type for different values of the exponent "p" (1-2-1).

$$\varepsilon^0_{yz}=y^*\frac{\partial w_b}{\partial y}+q^*\frac{\partial \theta}{\partial y},\ \varepsilon^3_{yz}=\frac{\partial \theta}{\partial y},\ \varepsilon^4_{yz}=\frac{\partial w_b}{\partial y}$$
$$\varepsilon^0_{xz}=y^*\frac{\partial w_b}{\partial x}+q^*\frac{\partial \theta}{\partial x},\ \varepsilon^3_{xz}=\frac{\partial \theta}{\partial x},\ \varepsilon^4_{xz}=\frac{\partial w_b}{\partial x}$$
$$\varepsilon^0_{xy}=\frac{\partial v}{\partial x}+\frac{\partial u}{\partial y},\ \varepsilon^1_{xy}=2y^{**}\frac{\partial^2 w_b}{\partial x\partial y}+2q^*\frac{\partial^2 \theta}{\partial x\partial y}-2\frac{\partial^2 w_s}{\partial x\partial y},\ \varepsilon^2_{xy}=2\frac{\partial^2 w_b}{\partial x\partial y} \tag{7a-p}$$

For the FG sandwich plates, the stress–strain relationships for plane-stress state including the thermal effects can be expressed as:

$$\begin{Bmatrix}\sigma_{xx}\\ \sigma_{yy}\\ \sigma_{zz}\\ \tau_{yz}\\ \tau_{xz}\\ \tau_{xy}\end{Bmatrix}^{(k)}=\begin{bmatrix}Q_{11} & Q_{12} & Q_{13} & 0 & 0 & 0\\ Q_{21} & Q_{22} & Q_{23} & 0 & 0 & 0\\ Q_{31} & Q_{32} & Q_{33} & 0 & 0 & 0\\ 0 & 0 & 0 & Q_{44} & 0 & 0\\ 0 & 0 & 0 & 0 & Q_{55} & \\ 0 & 0 & 0 & 0 & 0 & Q_{66}\end{bmatrix}^{(k)}\begin{Bmatrix}\varepsilon_{xx}-\alpha T\\ \varepsilon_{yy}-\alpha T\\ \varepsilon_{zz}-\alpha T\\ \gamma_{yz}\\ \gamma_{xz}\\ \gamma_{xy}\end{Bmatrix}^{(k)} \tag{8}$$

in which, $\sigma=\{\sigma_{xx},\sigma_{yy},\sigma_{zz},\ \tau_{yz},\tau_{xz},\tau_{xy}\}^{\mathrm{T}}$ and $\varepsilon=\{\varepsilon_{xx},\varepsilon_{yy},\ \varepsilon_{zz},\varepsilon_{yz},\varepsilon_{xz},\ \varepsilon_{xy}\}^{\mathrm{T}}$ are the stresses and the strain vectors with respect to the plate coordinate system; $\overline{T}=\{T,T,T,0,0,0\}^T$ is the temperature distribution vector. The Q_{ij} expressions in terms of engineering constants are given below:

$$Q_{11(z)}=Q_{22(z)}=Q_{33(z)}=\frac{E(z)}{(1-\nu^2)}$$
$$Q_{12(z)}=Q_{13(z)}=Q_{23(z)}=\frac{E(z)\nu}{(1-\nu^2)} \tag{9a-c}$$
$$Q_{44(z)}=Q_{55(z)}=Q_{66(z)}=\frac{E(z)}{2(1+\nu)}$$

The modulus $E(z), G(z)=\frac{E(z)}{2(1+\nu)}$ and the elastic coefficients $Q_{ij}(z)$ and the thermal expansion coefficients "$\alpha_{(Z)}$" vary through the thickness according to Eq. (1).

The generalized temperature field which varies through the thickness of the plate can be expressed as follows:

$$T(x,y,z)=T_1(x,y)+\frac{z}{h}T_2(x,y)+\frac{\Psi(z)}{h}T_3(x,y) \tag{10}$$

where T_1, T_2 and T_3 are thermal loads.

Note that in Eq. (10), the function of the nonlinear term is independent of the shape functions of the displacement field (see Eq. (4a-c)). The temperature distribution vector is given as:

$$\overline{T}=\overline{T}_1+\frac{z}{h}\overline{T}_2+\frac{\Psi(z)}{h}\overline{T}_3 \tag{11}$$

where

$$\overline{T}_n = \begin{bmatrix} T_n \\ T_n \\ T_n \\ 0 \\ 0 \\ 0 \end{bmatrix} \quad (n = 1,2,3) \tag{12}$$

2.4. Principle of virtual works (PVW)

The PVW is used for the thermoelastic bending problem of any plate. Also it can be used to study the considered FG sandwich plates. The principle is expressed as:

$$\delta U + \delta V = 0 \tag{13}$$

where δU is the virtual strain energy, δV is the external virtual works due to an external load applied to the plate. Them can be written as:

$$\delta U = \int_V \left(\sigma_{xx}\delta\varepsilon_{xx} + \sigma_{yy}\delta\varepsilon_{yy} + \sigma_{zz}\delta\varepsilon_{zz} + \tau_{yz}\delta\gamma_{yz} + \tau_{xz}\delta\gamma_{xz} + \tau_{xy}\delta\gamma_{xy}\right)dV \tag{14}$$

$$\delta V = -\int_\Omega q\delta\bar{w}d\Omega \tag{15}$$

In this paper only considers thermal loads, so the effect of the mechanical load of the above equation is deleted. Finally, the Eq. (13) is expressed as:

$$\left[\int_{-h/2}^{h/2}\left\{\int_\Omega \left[\sigma_{xx}\delta\varepsilon_{xx} + \sigma_{yy}\delta\varepsilon_{yy} + \sigma_{zz}\delta\varepsilon_{zz} + \tau_{yz}\delta\gamma_{yz} + \tau_{xz}\delta\gamma_{xz} + \tau_{xy}\delta\gamma_{xy}\right]dxdy\right\}dz\right] = 0 \tag{16}$$

$$\int_\Omega \left(N_1\delta\varepsilon^0_{xx} + M_1\delta\varepsilon^1_{xx} + P_1\delta\varepsilon^2_{xx} + N_2\delta\varepsilon^0_{yy} + M_2\delta\varepsilon^1_{yy} + P_2\delta\varepsilon^2_{yy} + R_3\delta\varepsilon^5_{zz} + N_4\delta\gamma^0_{yz} + Q_4\delta\gamma^3_{yz} + K_4\delta\gamma^4_{yz} + N_5\delta\gamma^0_{xz} + Q_5\delta\gamma^3_{xz} + K_5\delta\gamma^4_{xz} + N_6\delta\gamma^0_{xy} + M_6\delta\gamma^1_{xy} + P_6\delta\gamma^2_{xy}\right)dxdy = 0 \tag{17}$$

where N_i, M_i, P_i, Q_i and K_i are the resultants of the following integrations:

$$\{N_i, M_i, P_i\} = \sum_{k=1}^{3}\left[\int_{h_k}^{h_{k+1}} Q^{(k)}_{ij}\varepsilon^{(k)}_j\{1, z, f(z)\}dz\right] - \left\{N^T_i, M^T_i, P^T_i\right\}, \ (i=1,2)$$

$$\{N_6, M_6, P_6\} = \sum_{k=1}^{3}\left[\int_{h_k}^{zh_{k+1}} Q^{(k)}_{6j}\varepsilon^{(k)}_j\{1, z, f(z)\}dz\right],$$

$$\{N_i\} = \sum_{k=1}^{3}\left[\int_{h_k}^{zh_{k+1}} Q^{(k)}_{ij}\varepsilon^{(k)}_j dz\right], (i=4,5)$$

$$\{Q_i, K_i\} = \sum_{k=1}^{3}\left[\int_{h_k}^{h_{k+1}} Q^{(k)}_{ij}\varepsilon^{(k)}_j\{g(z), f'(z)\}dz\right], \ (i=4,5)$$

$$\{R_i\} = \sum_{k=1}^{3}\left[\int_{h_k}^{zh_{k+1}} Q^{(k)}_{ij}\varepsilon^{(k)}_j g\prime(z)dz\right] - R^T_i, \ (i=3)$$

$$\left\{N^T_i, M^T_i, P^T_i\right\} = \sum_{k=1}^{3}\left[\int_{h_k}^{h_{k+1}} \alpha^{(k)}_{(z)}Q^{(k)}_{ij}\overline{T}\{1, z, f(z)\}dz\right], \ (i=1,2)$$

$$\left\{R^T_i\right\} = \sum_{k=1}^{3}\left[\int_{h_k}^{h_{k+1}} \alpha^{(k)}_{(z)}Q^{(k)}_{ij}\overline{T}g'(z)dz\right], \ (i=3) \tag{18a-g}$$

2.5. Plate governing equations

Using the generalized displacement–strain relations (Eqs. (6a-f) and (7a-p)) and stress–strain relations (Eq. (8)), and integrating by parts and applying the fundamental lemma of variational calculus and collecting the coefficients of δu, δv, δw_b, δw_s, $\delta\theta$ in Eq. (17), the governing equations are obtained as:

$$\begin{aligned}
\delta u: &\quad \frac{\partial N_1}{\partial x} + \frac{\partial N_6}{\partial y} = 0\\
\delta v: &\quad \frac{\partial N_2}{\partial y} + \frac{\partial N_6}{\partial x} = 0\\
\delta w_b: &-y^{**}\left(\frac{\partial^2 M_1}{\partial x^2} + \frac{\partial^2 M_2}{\partial y^2} + 2\frac{\partial^2 M_6}{\partial x\partial y}\right) + y^*\left(\frac{\partial N_5}{\partial x} + \frac{\partial N_4}{\partial y}\right)\\
&- \frac{\partial^2 P_1}{\partial x^2} - \frac{\partial^2 P_2}{\partial y^2} - 2\frac{\partial^2 P_6}{\partial x\partial y} + \frac{\partial K_5}{\partial x} + \frac{\partial K_4}{\partial y} = 0\\
\delta w_s: &\quad \frac{\partial^2 M_1}{\partial x^2} + \frac{\partial^2 M_2}{\partial y^2} + 2\frac{\partial^2 M_6}{\partial x\partial y} = 0\\
\delta\theta: &-q^*\left(\frac{\partial^2 M_1}{\partial x^2} + \frac{\partial^2 M_2}{\partial y^2} + 2\frac{\partial^2 M_6}{\partial x\partial y} - \frac{\partial N_4}{\partial y} - \frac{\partial N_5}{\partial x}\right)\\
&+ \frac{\partial Q_4}{\partial y} + \frac{\partial Q_5}{\partial x} - R_3 = 0
\end{aligned} \tag{19a-e}$$

By substituting the stress–strain relations into the definitions of force and moment resultants given in Eq. (18a-g) the following constitutive equations are obtained:

$$\begin{aligned}
N_i &= A_{ij}\varepsilon^0_j + B_{ij}\varepsilon^1_j + C_{ij}\varepsilon^2_j + D_{ij}\varepsilon^3_j + E_{ij}\varepsilon^4_j + F_{ij}\varepsilon^5_j - A^*_{ij}\overline{T}_1\\
&\quad - B^*_{ij}\overline{T}^*_2 - C^*_{ij}\overline{T}^*_3, \quad (i=1,2)\\
N_i &= A_{ij}\varepsilon^0_j + B_{ij}\varepsilon^1_j + C_{ij}\varepsilon^2_j + D_{ij}\varepsilon^3_j + E_{ij}\varepsilon^4_j + F_{ij}\varepsilon^5_j, \quad (i=4,5,6)\\
M_i &= B_{ij}\varepsilon^0_j + G_{ij}\varepsilon^1_j + H_{ij}\varepsilon^2_j + I_{ij}\varepsilon^3_j + J_{ij}\varepsilon^4_j + K'_{ij}\varepsilon^5_j - B^*_{ij}\overline{T}_1 - G^*_{ij}\overline{T}^*_2 - H^*_{ij}\overline{T}^*_3,\\
&\quad (i=1,2)\\
M_i &= B_{ij}\varepsilon^0_j + G_{ij}\varepsilon^1_j + H_{ij}\varepsilon^2_j + I_{ij}\varepsilon^3_j + J_{ij}\varepsilon^4_j, \quad (i=6)\\
P_i &= C_{ij}\varepsilon^0_j + H_{ij}\varepsilon^1_j + L_{ij}\varepsilon^2_j + M'_{ij}\varepsilon^3_j + N'_{ij}\varepsilon^4_j + O_{ij}\varepsilon^5_j - C^{**}_{ij}\overline{T}_1\\
&\quad - H^{**}_{ij}\overline{T}^*_2 - L^{**}_{ij}\overline{T}^*_3, \quad (i=1,2)\\
P_i &= C_{ij}\varepsilon^0_j + H_{ij}\varepsilon^1_j + L_{ij}\varepsilon^2_j + M'_{ij}\varepsilon^3_j + N'_{ij}\varepsilon^4_j + O_{ij}\varepsilon^5_j, \quad (i=6)\\
Q_i &= D_{ij}\varepsilon^0_j + I_{ij}\varepsilon^1_j + M_{ij}\varepsilon^2_j + P'_{ij}\varepsilon^3_j + Q'_{ij}\varepsilon^4_j + R'_{ij}\varepsilon^5_j, \quad (i=4,5)\\
K_i &= E_{ij}\varepsilon^0_j + J_{ij}\varepsilon^1_j + N'_{ij}\varepsilon^2_j + Q'_{ij}\varepsilon^3_j + S_{ij}\varepsilon^4_j + T_{ij}\varepsilon^5_j, \quad (i=4,5)\\
R_i &= F_{ij}\varepsilon^0_j + K'_{ij}\varepsilon^1_j + O_{ij}\varepsilon^2_j + R'_{ij}\varepsilon^3_j + T_{ij}\varepsilon^4_j + U\varepsilon^5_j - F^*_{ij}\overline{T}_1 - K'^*_{ij}\overline{T}^*_2 - O^*_{ij}\overline{T}^*_3,\\
&\quad (i=3)
\end{aligned} \tag{20a-i}$$

where

$$(A_{ij}, B_{ij}, C_{ij}, D_{ij}, E_{ij}, F_{ij}) = \sum_{k=1}^{3}\int_{h_k}^{h_{k+1}} Q^{(k)}_{ij(z)}(1, z, f(z), g(z), f'(z), g'(z))dz$$

$$(G_{ij}, H_{ij}, I_{ij}, J_{ij}, K'_{ij}) = \sum_{k=1}^{3}\int_{h_k}^{h_{k+1}} Q^{(k)}_{ij(z)}(z^2, zf(z), zg(z), zf'(z), zg'(z))dz$$

$$(L_{ij}, M'_{ij}, N'_{ij}, O_{ij}) = \sum_{k=1}^{3}\int_{h_k}^{h_{k+1}} Q^{(k)}_{ij(z)}(f^2(z), f(z)g(z), f(z)f'(z), f(z)g'(z))dz$$

$$(P'_{ij}, Q'_{ij}, R'_{ij}) = \sum_{k=1}^{3}\int_{h_k}^{h_{k+1}} Q^{(k)}_{ij(z)}(g^2(z), g(z)f'(z), g(z)g'(z))dz$$

$$(S_{ij}, T_{ij}) = \sum_{k=1}^{3}\int_{h_k}^{h_{k+1}} Q^{(k)}_{ij(z)}(f'^2(z), f'(z)g'(z))dz$$

$$(U_{ij}) = \sum_{k=1}^{3}\int_{h_k}^{h_{k+1}} Q^{(k)}_{ij(z)}(g'^2(z))dz$$

$$(A^*_{ij}, B^*_{ij}, C^*_{ij}, F^*_{ij}) = \sum_{k=1}^{3}\int_{h_k}^{h_{k+1}} \alpha^{(k)}_{(z)} Q^{(k)}_{ij(z)}(1, z, \Psi(z), g'(z))dz$$

$$\left(G^*_{ij}, H^*_{ij}, K'^*_{ij}\right) = \sum_{k=1}^{3}\int_{h_k}^{h_{k+1}} \alpha^{(k)}_{(z)} Q^{(k)}_{ij(z)}(z^2, z\Psi(z), zg'(z))dz$$

$$(O^*_{ij}) = \sum_{k=1}^{3}\int_{h_k}^{h_{k+1}} \alpha^{(k)}_{(z)} Q^{(k)}_{ij(z)}(g'(z)\Psi(z))dz$$

$$(C^{**}_{ij}, H^{**}_{ij}, L^{**}_{ij}) = \sum_{k=1}^{3}\int_{h_k}^{h_{k+1}} \alpha^{(k)}_{(z)} Q^{(k)}_{ij(z)}(f(z), zf(z), f(z)\Psi(z))dz$$

$$\overline{T}^*_n = \overline{T}_n/h \ (n = 2,3) \tag{21a-k}$$

In what follows, the problem under consideration is solved for the simply supported boundary conditions and they are given at all four edges as follows:

$$N_1 = M_1 = P_1 = v = w_b = w_s = \frac{\partial w_b}{\partial y} = \theta \text{ at } x = 0, a$$
$$N_2 = M_2 = P_2 = u = w_b = w_s = \frac{\partial w_b}{\partial x} = \theta \text{ at } y = 0, b \tag{22a, b}$$

3. Solution procedure

For the analytical solution of the governing Eq. (19a-e), the Navier method, based on double Fourier series can be used considering the specified boundary conditions. Using Navier's procedure, the solution of the displacement variables satisfying the above boundary conditions can be expressed in the following Fourier series:

$$u(x,y) = \sum_{r=1}^{\infty}\sum_{s=1}^{\infty} U_{rs}\cos(\lambda x)\sin(\beta y), \quad 0 \leqslant x \leqslant a; \quad 0 \leqslant y \leqslant b \tag{23a}$$

$$v(x,y) = \sum_{r=1}^{\infty}\sum_{s=1}^{\infty} V_{rs}\sin(\lambda x)\cos(\beta y), \quad 0 \leqslant x \leqslant a; \quad 0 \leqslant y \leqslant b \tag{23b}$$

$$w_b(x,y) = \sum_{r=1}^{\infty}\sum_{s=1}^{\infty} W^b_{rs}\sin(\lambda x)\sin(\beta y), \quad 0 \leqslant x \leqslant a; \quad 0 \leqslant y \leqslant b \tag{23c}$$

$$w_s(x,y) = \sum_{r=1}^{\infty}\sum_{s=1}^{\infty} W^s_{rs}\sin(\lambda x)\sin(\beta y), \quad 0 \leqslant x \leqslant a; \quad 0 \leqslant y \leqslant b \tag{23d}$$

$$\theta(x,y) = \sum_{r=1}^{\infty}\sum_{s=1}^{\infty} \Theta_{rs}\sin(\lambda x)\sin(\beta y), \quad 0 \leqslant x \leqslant a; \quad 0 \leqslant y \leqslant b \tag{23e}$$

where

$$\lambda = \frac{r\pi}{a}, \quad \beta = \frac{s\pi}{b} \tag{24}$$

The transverse thermal loads T_1, T_2, T_3 are also expanded with double-Fourier sine series as:

$$T_i(x,y) = \sum_{r=1}^{\infty}\sum_{s=1}^{\infty} T^i_{mn}\sin(\lambda x)\sin(\beta y), (i = 1,2,3) \tag{25}$$

where

$$T^i_{mn} = \widehat{T}_i; \text{ for sinusoidally distributed thermal load} \tag{26a}$$

$$T^i_{mn} = \frac{16\widehat{T}_i}{rs\pi^2}; \text{ for uniformly distributed thermal load} \tag{26b}$$

From Eq. (20a-i), it can be noticed that for N_i, M_i, P_i, Q_i, K_i, and R_i, the variables depending on x and y are the strains, $\varepsilon^b_j(b = 0, \ldots, 5)$. Therefore, the expressions in each of the plate governing Eq. (19a-e), for example $\frac{\partial^2 N_i}{\partial x^2}, \frac{\partial^2 M_i}{\partial x^2}$, can be expressed as follows:

$$\tfrac{\partial^2(N_i, M_i)}{\partial x^2} = (A_{ij}, B_{ij})\begin{bmatrix}\lambda^3 & 0 & 0 & 0 & 0\\ 0 & \lambda^2\beta & 0 & 0 & 0\\ 0 & 0 & 0 & 0 & 0\\ 0 & 0 & -y^*\lambda^2\beta & 0 & -q^*\lambda^2\beta\\ 0 & 0 & -y^*\lambda^3 & 0 & -q^*\lambda^3\\ -\lambda^2\beta & -\lambda^3 & 0 & 0 & 0\end{bmatrix}\begin{bmatrix}U_{rs'}\\ V_{rs'}\\ W^s_{rs'}\\ W^b_{rs'}\\ \Theta_{rs'}\end{bmatrix}^T \times \begin{Bmatrix}SS\\ SS\\ SS\\ SC\\ CS\\ CC\end{Bmatrix} +$$

$$(B_{ij}, G_{ij})\begin{bmatrix}0 & 0 & y^{**}\lambda^4 & -\lambda^4 & q^*\lambda^4\\ 0 & 0 & y^{**}\lambda^2\beta^2 & -\lambda^2\beta^2 & q^*\lambda^2\beta^2\\ 0 & 0 & 0 & 0 & 0\\ 0 & 0 & 0 & 0 & 0\\ 0 & 0 & 0 & 0 & 0\\ 0 & 0 & -y^{**}2\lambda^3\beta & +2\lambda^3\beta & -2q^*\lambda^3\beta\end{bmatrix}\begin{bmatrix}U_{rs'}\\ V_{rs'}\\ W^s_{rs'}\\ W^b_{rs'}\\ \Theta_{rs'}\end{bmatrix}^T \times \begin{Bmatrix}SS\\ SS\\ SS\\ SC\\ CS\\ CC\end{Bmatrix} +$$

$$(C_{ij}, H_{ij})\begin{bmatrix}0 & 0 & \lambda^4 & 0 & 0\\ 0 & 0 & \lambda^2\beta^2 & 0 & 0\\ 0 & 0 & 0 & 0 & 0\\ 0 & 0 & 0 & 0 & 0\\ 0 & 0 & -2\lambda^3\beta & 0 & 0\end{bmatrix}\begin{bmatrix}U_{rs'}\\ V_{rs'}\\ W^s_{rs'}\\ W^b_{rs'}\\ \Theta_{rs'}\end{bmatrix}^T \times \begin{Bmatrix}SS\\ SS\\ SS\\ SC\\ CS\\ CC\end{Bmatrix} +$$

$$(D_{ij}, I_{ij})\begin{bmatrix}0 & 0 & 0 & 0 & 0\\ 0 & 0 & 0 & 0 & 0\\ 0 & 0 & 0 & 0 & 0\\ 0 & 0 & 0 & 0 & -\lambda^2\beta\\ 0 & 0 & 0 & 0 & -\lambda^3\\ 0 & 0 & 0 & 0 & 0\end{bmatrix}\begin{bmatrix}U_{rs'}\\ V_{rs'}\\ W^s_{rs'}\\ W^b_{rs'}\\ \Theta_{rs'}\end{bmatrix}^T \times \begin{Bmatrix}SS\\ SS\\ SS\\ SC\\ CS\\ CC\end{Bmatrix} +$$

$$(E_{ij}, J_{ij})\begin{bmatrix}0 & 0 & 0 & 0 & 0\\ 0 & 0 & 0 & 0 & 0\\ 0 & 0 & 0 & 0 & 0\\ 0 & 0 & -\lambda^2\beta & 0 & 0\\ 0 & 0 & -\lambda^3 & 0 & 0\\ 0 & 0 & 0 & 0 & 0\end{bmatrix}\begin{bmatrix}U_{rs'}\\ V_{rs'}\\ W^s_{rs'}\\ W^b_{rs'}\\ \Theta_{rs'}\end{bmatrix}^T \times \begin{Bmatrix}SS\\ SS\\ SS\\ SC\\ CS\\ CC\end{Bmatrix} +$$

$$\left(F_{ij}, K'_{ij}\right)\begin{bmatrix}0 & 0 & 0 & 0 & 0\\ 0 & 0 & 0 & 0 & 0\\ 0 & 0 & 0 & 0 & -\lambda^2\\ 0 & 0 & 0 & 0 & 0\\ 0 & 0 & 0 & 0 & 0\\ 0 & 0 & 0 & 0 & 0\end{bmatrix}\begin{bmatrix}U_{rs'}\\ V_{rs'}\\ W^s_{rs'}\\ W^b_{rs'}\\ \Theta_{rs'}\end{bmatrix}^T \times \begin{Bmatrix}SS\\ SS\\ SS\\ SC\\ CS\\ CC\end{Bmatrix} - \frac{\partial^2(N^T_i, M^T_i)}{\partial x^2} \tag{27}$$

where SS = $\sin(\lambda x)\sin(\beta y)$, SC = $\sin(\lambda x)\cos(\beta y)$ and so for, and the elements of the 6×5 matrices are the coefficients obtained after taking the second derivation of the strains expression in the Eq. (20a-i). As is known, the generalized strains are expressions as a function of the 5 unknowns, described in Eqs. (4a-c) and (23a-e).

The 6×5 matrices associated with $\frac{\partial^2 M_i}{\partial x^2}$ in Eq. (27), is called $\overline{M}^{2,b}_x(b = 0, \ldots, 5)$.

The symbols used in $\overline{M}^{a,b}_v$ are as follow: the first upper and lower (a, v) indicates the derivative (second derivative with respect to x, in the example), and the second upper character, b, indicates that the derivative is associates with the strain $\varepsilon^b_j(b = 0, \ldots, 5)$. For example, $\overline{M}^{2,0}_x$ is (see Eq. (27)):

$$\overline{M}^{2,0}_x = \begin{bmatrix}\alpha^3 & 0 & 0 & 0 & 0\\ 0 & \alpha^2\beta & 0 & 0 & 0\\ 0 & 0 & 0 & 0 & 0\\ 0 & 0 & -y^*\alpha^2\beta & 0 & -q^*\alpha^2\beta\\ 0 & 0 & -y^*\alpha^3 & 0 & -q^*\alpha^3\\ -\alpha^2\beta & -\alpha^3 & 0 & 0 & 0\end{bmatrix} \tag{28}$$

In summary, substituting Eqs. (23a-e) and (25) into Eq. (19a-e), the following equations are obtained,

$$K_{ij}\Delta_j = \{F\} \quad (i,j = 1,\ldots\ldots,5) \text{ and } (K_{ij} = K_{ji}) \tag{29}$$

where Δ_j is the column vector of coefficients $\left\{U_{rs}V_{rs}W^b_{rs}W^s_{rs}\Theta_{rs}\right\}$ and $\{F\} = \{F_1 \quad F_2 \quad F_3 \quad F_4 \quad F_5\}^T$ is the column vector of coefficients of the thermal load:

$$F_1 = \lambda\left(A^*_{1j}\widehat{T}_1 + B^*_{1j}\frac{\widehat{T}_2}{h} + C^*_{1j}\frac{\widehat{T}_3}{h}\right)\{T^u\} \tag{30a}$$

$$F_2 = \beta\left(A^*_{2j}\widehat{T}_1 + B^*_{2j}\frac{\widehat{T}_2}{h} + C^*_{2j}\frac{\widehat{T}_3}{h}\right)\{T^u\} \tag{30b}$$

$$\begin{aligned} F_3 = {} & y^{**}\lambda^2\left(B^*_{1j}\widehat{T}_1 + G^*_{1j}\frac{\widehat{T}_2}{h} + H^*_{1j}\frac{\widehat{T}_3}{h}\right)\{T^u\} \\ & + y^{**}\beta^2\left(B^*_{2j}\widehat{T}_1 + G^*_{2j}\frac{\widehat{T}_2}{h} + H^*_{2j}\frac{\widehat{T}_3}{h}\right)\{T^u\} \\ & + \lambda^2\left(C^{**}_{1j}\widehat{T}_1 + H^{**}_{1j}\frac{\widehat{T}_2}{h} + L^{**}_{1j}\frac{\widehat{T}_3}{h}\right)\{T^u\} \\ & + \beta^2\left(C^{**}_{2j}\widehat{T}_1 + H^{**}_{2j}\frac{\widehat{T}_2}{h} + L^{**}_{2j}\frac{\widehat{T}_3}{h}\right)\{T^u\} \end{aligned} \tag{30c}$$

$$\begin{aligned} F_4 = {} & -\lambda^2\left(B^*_{1j}\widehat{T}_1 + G^*_{1j}\frac{\widehat{T}_2}{h} + H^*_{1j}\frac{\widehat{T}_3}{h}\right)\{T^u\} \\ & - \beta^2\left(B^*_{2j}\widehat{T}_1 + G^*_{2j}\frac{\widehat{T}_2}{h} + H^*_{2j}\frac{\widehat{T}_3}{h}\right)\{T^u\} \end{aligned} \tag{30d}$$

$$\begin{aligned} F_5 = {} & q^*\lambda^2\left(B^*_{1j}\widehat{T}_1 + G^*_{1j}\frac{\widehat{T}_2}{h} + H^*_{1j}\frac{\widehat{T}_3}{h}\right)\{T^u\} \\ & + q^*\beta^2\left(B^*_{2j}\widehat{T}_1 + G^*_{2j}\frac{\widehat{T}_2}{h} + H^*_{2j}\frac{\widehat{T}_3}{h}\right)\{T^u\} \\ & - \left(F^*_{3j}\widehat{T}_1 + K'^*_{3j}\frac{\widehat{T}_2}{h} + O^*_{3j}\frac{\widehat{T}_3}{h}\right)\{T^u\} \end{aligned} \tag{30e}$$

$$\{T^u\} = \{1 \quad 1 \quad 1 \quad 0 \quad 0 \quad 0\}^T \tag{30f}$$

Elements of K_{ij} in Eq. (29) can be obtained by using the matrices $\overline{M}^{a,b}_{v}$. All matrices of type $\overline{M}^{a,b}_{v}$, associated with the expressions of the plate governing Eq. (19a-e) are given in Appendix A.

4. Numerical results and discussions

In this section the results of the thermoelastic bending analysis of isotropic and FG sandwich plates are presented. The present results are obtained from the present new quasi-3D hybrid type HSDT with only 5 unknowns. The theory is formulated in such way that the thickness stretching effect is taken into account, i.e. the Koiter's recommendation regarding stretching effect of the plate [42] is obeyed. The isotropic plates are analyzed for validation purposes, since a quasi-exact solution (layerwise) based on CUF for this type of problem is given in Ref. [33]. The CUF is the best framework to assess any theory for plates. Various numerical examples for two types of FG sandwich plates with various exponents that specify the material variation profile through the thickness, "p", several aspect ratios "a/b" and different sandwich schemes are presented. Typical mechanical properties for metal and ceramics used in the numerical examples are listed in Table 1. The simply supported FG sandwich plates are subjected to a bi-sinusoidal thermal load. All results were obtained considering a side-to-thickness ratio $a/h = 10$. In this paper, the following dimensionless relations for the deflection and stresses of thermoelastic bending problem are used:

$$\begin{aligned} & \bar{w} = \frac{h}{\alpha_0\widehat{T}_2a^2}w\left(\frac{a}{2},\frac{b}{2}\right), \quad \bar{\sigma}_{xx} = \frac{h^2}{\alpha_0\widehat{T}_2E_0a^2}\sigma_{xx}\left(\frac{a}{2},\frac{b}{2},\frac{h}{2}\right), \\ & \bar{\tau}_{xz} = \frac{10h}{\alpha_0\widehat{T}_2E_0a}\tau_{xz}\left(0,\frac{b}{2},0\right) \\ & E_0 = 1\text{ GPa}, \quad \alpha_0 = 10^{-6}\,{}^\circ\text{C}^{-1} \end{aligned} \tag{31}$$

4.1. Isotropic plate

The deflection w and in-plane displacement u of one-layered isotropic square plates for several side-to-thickness ratios "a/h" are given in Tables 2 and 3, respectively. The considered plates, with total thickness $h = 1$ m, are simply supported. The plates are made of Al2024 with Young's modulus $E = 73$ GPa, Poisson's ratio $\nu = 0.3$ and thermal expansion coefficient $\alpha = 25 \times 10^{-6}$ 1/K. The isotropic plate is subjected to a temperature distribution that varies linearly across the thickness from $\widehat{T}_{top} = 1$ to $\widehat{T}_{bottom} = 0$. The present results are compared with solutions of several theories based on CUF [33]. From Table 2 it can be seen that the results of the deflection (mm) are lower than those predicted by the classical theories, such as FSDT and classical plate theory (CPT). However, the results show good agreement with the HSDTs that considered a thermo-mechanical analysis both partially and fully coupled. In Table 3 can be noted that the in plane displacements (mm) obtained by the present theory (in absolute value) overpredicts the results based on HSDTs in all cases. In Tables 2 and 3 it can be seen that the present results are close to the reference solutions for thick plates. For more details on the thermo-mechanical analysis of one-layered plates (the identification of acronyms that define various refined 2D models used in the abovementioned tables, the definition of the Q_{ij} expressions, etc.) is recommended to review the interesting work of Brischetto and Carrera [33].

4.2. FG sandwich plate A-type

Table 4 presents results of non-dimensional deflections $\bar{w}$ of FG sandwich square plates for various sandwich schemes and

Table 1
Material properties of the used FG sandwich plates.

Material	Properties		
	E (GPa)	α ($\times 10^{-6}$/°C)	ν
Metal: Ti–6A1–4V	66.2	10.3	1/3
Ceramic: ZrO_2	117	7.11	1/3

Table 2
Comparison of deflection w (mm) of one-layered isotropic square plates ($a = b$, $h = 1$ m, $\widehat{T}_1 = 0.5, \widehat{T}_2 = 1, \widehat{T}_3 = 0$).

Theory	a/h				
	2	5	10	50	100
Present	0.0057	0.0406	0.1650	4.1464	16.588
Ref. [33] (LD4 (⊖a))	0.0057	0.0403	0.1638	4.1154	16.464
Ref. [33] (LD4 (⊖c))	0.0054	0.0398	0.1633	4.1148	16.463
Ref. [33] (LD4 (TM))	0.0054	0.0398	0.1633	4.1148	16.463
Ref. [33] (LD2 (⊖a))	0.0053	0.0399	0.1634	4.1149	16.463
Ref. [33] (LD2 (⊖c))	0.0053	0.0399	0.1634	4.1149	16.463
Ref. [33] (LD2 (TM))	0.0053	0.0399	0.1634	4.1149	16.463
Ref. [33] (FSDT (⊖a))	0.0092	0.0578	0.2311	5.7785	23.114
Ref. [33] (FSDT (⊖c))	0.0092	0.0578	0.2311	5.7785	23.114
Ref. [33] (FSDT (TM))	0.0092	0.0578	0.2311	5.7785	23.114
Ref. [33] (CPT (⊖a))	0.0092	0.0578	0.2311	5.7785	23.114
Ref. [33] (CPT (⊖c))	0.0092	0.0578	0.2311	5.7785	23.114
Ref. [33] (CPT (TM))	0.0092	0.0578	0.2311	5.7785	23.114

Table 3
Comparison of in-plane displacement u (mm) of one-layered isotropic square plates ($a = b$, $h = 1$ m, $\hat{T}_1 = 0.5, \hat{T}_2 = 1, \hat{T}_3 = 0$).

Theory	a/h				
	2	5	10	50	100
Present	−0.0131	−0.0317	−0.0631	−0.3150	−0.6301
Ref. [33] (LD4 (⊖a))	−0.0125	−0.0269	−0.0522	−0.2587	−0.5173
Ref. [33] (LD4 (⊖c))	−0.0119	−0.0267	−0.0521	−0.2587	−0.5173
Ref. [33] (LD4 (TM))	−0.0103	−0.0259	−0.0517	−0.2586	−0.5172
Ref. [33] (LD2 (⊖a))	−0.0121	−0.0267	−0.0522	−0.2587	−0.5173
Ref. [33] (LD2 (⊖c))	−0.0107	−0.0259	−0.0517	−0.2586	−0.5172
Ref. [33] (LD2 (TM))	−0.0106	−0.0259	−0.0517	−0.2586	−0.5172
Ref. [33] (FSDT (⊖a))	−0.0145	−0.0363	−0.0726	−0.3631	−0.7261
Ref. [33] (FSDT (⊖c))	−0.0145	−0.0363	−0.0726	−0.3631	−0.7261
Ref. [33] (FSDT (TM))	−0.0145	−0.0363	−0.0726	−0.3631	−0.7261
Ref. [33] (CPT (⊖a))	−0.0145	−0.0363	−0.0726	−0.3631	−0.7261
Ref. [33] (CPT (⊖c))	−0.0145	−0.0363	−0.0726	−0.3631	−0.7261
Ref. [33] (CPT (TM))	−0.0145	−0.0363	−0.0726	−0.3631	−0.7261

exponents "p". The sandwich plate is subjected to a linear temperature distribution through the thickness ($\widehat{T}_3 = 0$). The present results are compared with solutions based on a refined HSDT [40] and HSDTs proposed by Reddy [43] (TSDT), Touratier [44] (SSDT) and Karama [45,46] (ESDT) which were reproduced by Tounsi et al. [40]. From this table it can be seen that the present results are lower than the other solutions proposed for comparison. The non-dimensional deflection increases as the exponent "p" increases. However, this effect decreases for higher values of the exponent "p". Table 5 presents results of non-dimensional deflections $\bar{w}$ of FG sandwich plates for different values of aspect ratio "a/b" and several sandwich schemes, considering an exponent $p = 3$. The sandwich plate is subjected to a linear temperature distribution through the thickness ($\widehat{T}_3 = 0$). The results are compared with HSDTs as in Table 4. For aspect ratios $a/b \geqslant 3$, the present results are higher than the other results. However, for aspect ratios $a/b < 3$ the opposite occurs. The value of the non-dimensional deflection decreases as the aspect ratio "a/b" increases. From Tables 4 and 5 it can be noticed that the stretching effect decreases the deflection results for aspect ratios $a/b < 3$. The aspect ratio "a/b" has a higher influence on the results than the exponent "p".

The results of non-dimensional axial stresses $\bar{\sigma}_{xx}$ of FG sandwich square plates for several values of exponent "p" and different sandwich schemes are presented in Table 6. The sandwich plate is subjected to a linear temperature distribution through the thickness ($\widehat{T}_3 = 0$). Table 6 presents results that are higher (in absolute value) than the other solutions due to the influence of the thickness stretching effect. The last column presents lower axial stress results because the sandwich scheme is rich in metal. For a given sandwich scheme, the axial stresses do not follow a specific pattern with respect to the exponent "p", in some cases increases (see "2-1-2") and in others the reverse is true (see "1-1-1").

Table 7 presents results of non-dimensional transverse shear stresses $\bar{\tau}_{xz}$ of FG sandwich square plates for several values of exponent "p" and different sandwich schemes. The results are compared with several HSDTs as mentioned previously. The sandwich plate is subjected to a distribution of both linear and nonlinear temperature ($\widehat{T}_3 = -100$). Note that this table was prepared by considering that the function of the nonlinear temperature distribution is equal to shear strain shape function of the displacement field, i.e., $f(z) = \Psi(z)$. It can be noticed that the results of all theories are different, except the solutions of the SSDT and refined shear deformation theory proposed by Tounsi et al. [40]. The reason is in the utilized sinusoidal shear strain shape functions. This difference in results can be attributed to the nonlinear term of the temperature field. Consequently, attention must be taken when further studies are carried out.

Table 4
Comparison of non-dimensional deflection $\bar{w}$ of FG sandwich square plates A-type ($a/h = 10$, $\hat{T}_1 = \hat{T}_3 = 0$, $\hat{T}_2 = 100$).

p	Theory	$\bar{w}$				
		1-2-2	1-1-1	1-2-1	2-1-2	2-2-1
0	Tounsi et al. [40] ($\varepsilon z = 0$)	0.544640	0.569801	0.556060	0.576238	0.576238
	SSDT ($\varepsilon z = 0$)	0.544640	0.569801	0.556060	0.576238	0.576238
	TSDT ($\varepsilon z = 0$)	0.544619	0.569796	0.556044	0.576240	0.576240
	ESDT ($\varepsilon z = 0$)	0.544662	0.569807	0.556076	0.576236	0.576236
	Present($\varepsilon z \neq 0$)	0.526933	0.552626	0.538460	0.559624	0.559624
1	Tounsi et al. [40] ($\varepsilon z = 0$)	0.573055	0.578804	0.577909	0.579503	0.582578
	SSDT ($\varepsilon z = 0$)	0.573055	0.578804	0.577909	0.579503	0.582578
	TSDT ($\varepsilon z = 0$)	0.573054	0.578809	0.577914	0.579510	0.582593
	ESDT ($\varepsilon z = 0$)	0.573056	0.578797	0.577903	0.579497	0.582564
	Present($\varepsilon z \neq 0$)	0.556137	0.562367	0.560767	0.563428	0.564971
2	Tounsi et al. [40] ($\varepsilon z = 0$)	0.577551	0.580037	0.580945	0.580018	0.584582
	SSDT ($\varepsilon z = 0$)	0.577551	0.580037	0.580945	0.580018	0.584582
	TSDT ($\varepsilon z = 0$)	0.577555	0.580045	0.580957	0.580025	0.584601
	ESDT ($\varepsilon z = 0$)	0.577547	0.580028	0.580933	0.580010	0.584562
	Present($\varepsilon z \neq 0$)	0.561155	0.563652	0.563663	0.564029	0.566078
3	Tounsi et al. [40] ($\varepsilon z = 0$)	0.578976	0.580412	0.581997	0.580181	0.585807
	SSDT ($\varepsilon z = 0$)	0.578976	0.580412	0.581997	0.580181	0.585807
	TSDT ($\varepsilon z = 0$)	0.578982	0.580421	0.582011	0.580188	0.585829
	ESDT ($\varepsilon z = 0$)	0.578970	0.580402	0.581982	0.580173	0.585783
	Present($\varepsilon z \neq 0$)	0.562797	0.563961	0.564439	0.564202	0.566687
4	Tounsi et al. [40] ($\varepsilon z = 0$)	0.579572	0.580574	0.582554	0.580249	0.586680
	SSDT ($\varepsilon z = 0$)	0.579572	0.580574	0.582554	0.580249	0.586680
	TSDT ($\varepsilon z = 0$)	0.579579	0.580584	0.582570	0.580257	0.586705
	ESDT ($\varepsilon z = 0$)	0.579565	0.580564	0.582537	0.580241	0.586655
	Present($\varepsilon z \neq 0$)	0.563490	0.564044	0.564738	0.564263	0.567126
5	Tounsi et al. [40] ($\varepsilon z = 0$)	0.579865	0.580663	0.582925	0.580282	0.587346
	SSDT ($\varepsilon z = 0$)	0.579865	0.580663	0.582925	0.580282	0.587346
	TSDT ($\varepsilon z = 0$)	0.579872	0.580673	0.582942	0.580290	0.587373
	ESDT ($\varepsilon z = 0$)	0.579858	0.580652	0.582907	0.580274	0.587319
	Present($\varepsilon z \neq 0$)	0.563830	0.564059	0.564891	0.564285	0.567472

Table 5
Comparison of non-dimensional deflection $\bar{w}$of FG sandwich rectangular plates A-type ($p = 3$, $a/h = 10$, $\hat{T}_1 = \hat{T}_3 = 0, \hat{T}_2 = 100$).

Scheme	Theory	$\bar{w}$				
		$a/b = 1$	$a/b = 2$	$a/b = 3$	$a/b = 4$	$a/b = 5$
1-2-2	Tounsi et al. [40] ($\varepsilon z = 0$)	0.578976	0.231560	0.115754	0.068070	0.044490
	SSDT ($\varepsilon z = 0$)	0.578976	0.231560	0.115754	0.068070	0.044490
	TSDT ($\varepsilon z = 0$)	0.578982	0.231566	0.115760	0.068076	0.044495
	ESDT ($\varepsilon z = 0$)	0.578970	0.231554	0.115749	0.068064	0.044484
	Present($\varepsilon z \neq 0$)	0.562797	0.231291	0.120773	0.075245	0.052706
1-1-1	Tounsi et al. [40] ($\varepsilon z = 0$)	0.580412	0.232119	0.116022	0.068217	0.044578
	SSDT ($\varepsilon z = 0$)	0.580412	0.232119	0.116022	0.068217	0.044578
	TSDT ($\varepsilon z = 0$)	0.580421	0.232128	0.116031	0.068226	0.044587
	ESDT ($\varepsilon z = 0$)	0.580402	0.232109	0.116012	0.068208	0.044568
	Present($\varepsilon z \neq 0$)	0.563961	0.231781	0.121037	0.075412	0.052822
1-2-1	Tounsi et al. [40] ($\varepsilon z = 0$)	0.581997	0.232730	0.116309	0.068370	0.044665
	SSDT ($\varepsilon z = 0$)	0.581997	0.232730	0.116309	0.068370	0.044665
	TSDT ($\varepsilon z = 0$)	0.582011	0.232745	0.116323	0.068384	0.044679
	ESDT ($\varepsilon z = 0$)	0.581982	0.232716	0.116294	0.068356	0.044651
	Present($\varepsilon z \neq 0$)	0.564439	0.232005	0.121174	0.075513	0.052903
2-1-2	Tounsi et al. [40] ($\varepsilon z = 0$)	0.580181	0.232033	0.115985	0.068200	0.044570
	SSDT ($\varepsilon z = 0$)	0.580181	0.232033	0.115985	0.068200	0.044570
	TSDT ($\varepsilon z = 0$)	0.580188	0.232041	0.115992	0.068207	0.044578
	ESDT ($\varepsilon z = 0$)	0.580173	0.232026	0.115977	0.068192	0.044563
	Present($\varepsilon z \neq 0$)	0.564202	0.231859	0.121061	0.075416	0.052816
2-2-1	Tounsi et al. [40] ($\varepsilon z = 0$)	0.585807	0.234213	0.117015	0.068757	0.044894
	SSDT ($\varepsilon z = 0$)	0.585807	0.234213	0.117015	0.068757	0.044894
	TSDT ($\varepsilon z = 0$)	0.585829	0.234235	0.117037	0.068780	0.044916
	ESDT ($\varepsilon z = 0$)	0.585783	0.234189	0.116992	0.068734	0.044872
	Present($\varepsilon z \neq 0$)	0.566687	0.232955	0.121690	0.075847	0.053145

Table 6
Comparison of non-dimensional axial stress $\bar{\sigma}_{xx}$ of FG sandwich square plates A-type ($a/h = 10$, $\hat{T}_1 = \hat{T}_3 = 0, \hat{T}_2 = 100$).

p	Theory	$\bar{\sigma}_{xx}$				
		1-2-2	1-1-1	1-2-1	2-1-2	2-2-1
0	Tounsi et al. [40] ($\varepsilon z = 0$)	−1.750776	−1.666252	−1.706108	−1.659815	−1.659815
	SSDT ($\varepsilon z = 0$)	−1.750776	−1.666252	−1.706108	−1.659815	−1.659815
	TSDT ($\varepsilon z = 0$)	−1.750827	−1.666262	−1.706145	−1.659810	−1.659810
	ESDT ($\varepsilon z = 0$)	−1.750721	−1.666239	−1.706067	−1.659822	−1.659822
	Present($\varepsilon z \neq 0$)	−1.854358	−1.728376	−1.789407	−1.716376	−1.716376
1	Tounsi et al. [40] ($\varepsilon z = 0$)	−1.674484	−1.664562	−1.650243	−1.670106	−1.619835
	SSDT ($\varepsilon z = 0$)	−1.674484	−1.664562	−1.650243	−1.670106	−1.619835
	TSDT ($\varepsilon z = 0$)	−1.674486	−1.664548	−1.650230	−1.670091	−1.619803
	ESDT ($\varepsilon z = 0$)	−1.674482	−1.664577	−1.650258	−1.670123	−1.619870
	Present($\varepsilon z \neq 0$)	−1.737710	−1.720419	−1.700455	−1.728314	−1.654704
2	Tounsi et al. [40] ($\varepsilon z = 0$)	−1.670218	−1.665247	−1.638341	−1.673313	−1.591812
	SSDT ($\varepsilon z = 0$)	−1.670218	−1.665247	−1.638341	−1.673313	−1.591812
	TSDT ($\varepsilon z = 0$)	−1.670208	−1.665228	−1.638316	−1.673296	−1.591770
	ESDT ($\varepsilon z = 0$)	−1.670228	−1.665268	−1.638370	−1.673332	−1.591860
	Present($\varepsilon z \neq 0$)	−1.729426	−1.719839	−1.680872	−1.732050	−1.612327
3	Tounsi et al. [40] ($\varepsilon z = 0$)	−1.670990	−1.664984	−1.630191	−1.674783	−1.572299
	SSDT ($\varepsilon z = 0$)	−1.670990	−1.664984	−1.630191	−1.674783	−1.572299
	TSDT ($\varepsilon z = 0$)	−1.670977	−1.664963	−1.630160	−1.674766	−1.572250
	ESDT ($\varepsilon z = 0$)	−1.671005	−1.665007	−1.630226	−1.674803	−1.572353
	Present($\varepsilon z \neq 0$)	−1.729593	−1.718533	−1.667695	−1.733664	−1.582788
4	Tounsi et al. [40] ($\varepsilon z = 0$)	−1.672177	−1.664402	−1.623673	−1.675585	−1.558042
	SSDT ($\varepsilon z = 0$)	−1.672177	−1.664402	−1.623673	−1.675585	−1.558042
	TSDT ($\varepsilon z = 0$)	−1.672161	−1.664380	−1.623639	−1.675567	−1.557989
	ESDT ($\varepsilon z = 0$)	−1.672194	−1.664427	−1.623712	−1.675605	−1.558100
	Present($\varepsilon z \neq 0$)	−1.730754	−1.717034	−1.657248	−1.734479	−1.561206
5	Tounsi et al. [40] ($\varepsilon z = 0$)	−1.673181	−1.663752	−1.618307	−1.676071	−1.547192
	SSDT ($\varepsilon z = 0$)	−1.673181	−1.663752	−1.618307	−1.676071	−1.547192
	TSDT ($\varepsilon z = 0$)	−1.673165	−1.663729	−1.618270	−1.676053	−1.547136
	ESDT ($\varepsilon z = 0$)	−1.673199	−1.663777	−1.618349	−1.676091	−1.547254
	Present($\varepsilon z \neq 0$)	−1.731829	−1.715591	−1.648682	−1.734929	−1.544796

4.3. FG sandwich plate B-type

The results of non-dimensional deflections $\bar{w}$ of FG sandwich square plates for several values of exponent "p" and different sandwich schemes are presented in Table 8. The sandwich plate is subjected to a linear temperature distribution through the thickness ($\hat{T}_3 = 0$). The results are compared with analytical results based on TSDT and HSDTs with thickness stretching effect

Table 7
Comparison of non-dimensional shear stress $\bar{\tau}_{xz}$ of FG sandwich square plates A-type ($a/h = 10$, $\hat{T}_1 = 0, \hat{T}_2 = 100, \hat{T}_3 = -100$, $f(z) = \Psi(z)$).

p	Theory	$\bar{\tau}_{xz}$				
		1-2-2	1-1-1	1-2-1	2-1-2	2-2-1
0	Tounsi et al. [40] ($\varepsilon z = 0$)	0.634840	0.593473	0.618198	0.593749	0.593749
	SSDT ($\varepsilon z = 0$)	0.634840	0.593473	0.618198	0.593749	0.593749
	TSDT ($\varepsilon z = 0$)	0.512863	0.483594	0.500740	0.485205	0.485205
	ESDT ($\varepsilon z = 0$)	0.711266	0.717537	0.752081	0.715644	0.715644
	Present($\varepsilon z \neq 0$)	1.030120	0.968793	1.005739	0.971823	0.971823
1	Tounsi et al. [40] ($\varepsilon z = 0$)	0.556468	0.506552	0.510904	0.503367	0.462590
	SSDT ($\varepsilon z = 0$)	0.556468	0.506552	0.510904	0.503367	0.462590
	TSDT ($\varepsilon z = 0$)	0.452706	0.412275	0.415599	0.409890	0.376218
	ESDT ($\varepsilon z = 0$)	0.673909	0.613190	0.618781	0.609017	0.560375
	Present($\varepsilon z \neq 0$)	0.911134	0.833192	0.839726	0.828390	0.763771
2	Tounsi et al. [40] ($\varepsilon z = 0$)	0.515247	0.457581	0.463304	0.448325	0.425693
	SSDT ($\varepsilon z = 0$)	0.515247	0.457581	0.463304	0.448325	0.425693
	TSDT ($\varepsilon z = 0$)	0.419431	0.371598	0.376435	0.364374	0.345855
	ESDT ($\varepsilon z = 0$)	0.623600	0.555218	0.561816	0.543545	0.516221
	Present($\varepsilon z \neq 0$)	0.846399	0.754851	0.764361	0.739280	0.704632
3	Tounsi et al. [40] ($\varepsilon z = 0$)	0.485538	0.432335	0.439671	0.419756	0.417906
	SSDT ($\varepsilon z = 0$)	0.485538	0.432335	0.439671	0.419756	0.417906
	TSDT ($\varepsilon z = 0$)	0.395048	0.350601	0.356867	0.340784	0.339606
	ESDT ($\varepsilon z = 0$)	0.587968	0.525380	0.533729	0.509509	0.506632
	Present($\varepsilon z \neq 0$)	0.799046	0.714227	0.726674	0.692856	0.692412
4	Tounsi et al. [40] ($\varepsilon z = 0$)	0.462874	0.420409	0.428492	0.405887	0.416720
	SSDT ($\varepsilon z = 0$)	0.462874	0.420409	0.428492	0.405887	0.416720
	TSDT ($\varepsilon z = 0$)	0.376357	0.340633	0.347598	0.329301	0.338828
	ESDT ($\varepsilon z = 0$)	0.560929	0.511364	0.520457	0.493037	0.504883
	Present($\varepsilon z \neq 0$)	0.762630	0.695081	0.708860	0.670349	0.690747
5	Tounsi et al. [40] ($\varepsilon z = 0$)	0.445532	0.415369	0.423636	0.399587	0.416587
	SSDT ($\varepsilon z = 0$)	0.445532	0.415369	0.423636	0.399587	0.416587
	TSDT ($\varepsilon z = 0$)	0.362034	0.336364	0.343575	0.324042	0.338917
	ESDT ($\varepsilon z = 0$)	0.540270	0.505531	0.514681	0.485623	0.504398
	Present($\varepsilon z \neq 0$)	0.734637	0.687080	0.701195	0.660188	0.690685

Table 8
Comparison of non-dimensional deflection $\bar{w}$ of FG sandwich square plates B-type ($a/h = 10$, $\hat{T}_1 = \hat{T}_3 = 0$, $\hat{T}_2 = 100$).

p	Theory	$\bar{w}$				
		1-0-1	1-1-1	1-2-1	2-1-2	2-2-1
0	Houri et al. [39] ($\varepsilon z \neq 0$)	0.461634	0.461634	0.461634	0.461634	0.461634
	Zenkour et al. [13] ($\varepsilon z \neq 0$)	0.461634	0.461634	0.461634	0.461634	0.461634
	Zenkour et al. [13] ($\varepsilon z = 0$)	0.480262	0.480262	0.480262	0.480262	0.480262
	TSDT ($\varepsilon z = 0$)	0.480262	0.480262	0.480262	0.480262	0.480262
	Present($\varepsilon z \neq 0$)	0.461622	0.461622	0.461622	0.461622	0.461622
1	Houri et al. [39] ($\varepsilon z \neq 0$)	0.614565	0.586124	0.563416	0.599933	0.573327
	Zenkour et al. [13] ($\varepsilon z \neq 0$)	0.614565	0.586124	0.563416	0.599933	0.573327
	Zenkour et al. [13] ($\varepsilon z = 0$)	0.636916	0.606292	0.582342	0.621098	0.592604
	TSDT ($\varepsilon z = 0$)	0.636891	0.606256	0.582302	0.621067	0.592568
	Present($\varepsilon z \neq 0$)	0.614549	0.586131	0.563439	0.599926	0.573338
2	Houri et al. [39] ($\varepsilon z \neq 0$)	0.647135	0.618046	0.590491	0.633340	0.601843
	Zenkour et al. [13] ($\varepsilon z \neq 0$)	0.647135	0.618046	0.590491	0.633340	0.601843
	Zenkour et al. [13] ($\varepsilon z = 0$)	0.671503	0.639361	0.609875	0.656142	0.621581
	TSDT ($\varepsilon z = 0$)	0.671486	0.639325	0.609829	0.656115	0.621544
	Present($\varepsilon z \neq 0$)	0.647094	0.618037	0.590512	0.633310	0.601847
3	Houri et al. [39] ($\varepsilon z \neq 0$)	0.658153	0.631600	0.602744	0.646475	0.614121
	Zenkour et al. [13] ($\varepsilon z \neq 0$)	0.658153	0.631600	0.602744	0.646475	0.614121
	Zenkour et al. [13] ($\varepsilon z = 0$)	0.683572	0.653671	0.622467	0.670275	0.634175
	TSDT ($\varepsilon z = 0$)	0.683560	0.653638	0.622420	0.670253	0.634139
	Present($\varepsilon z \neq 0$)	0.658099	0.631579	0.602760	0.646428	0.614117
4	Houri et al. [39] ($\varepsilon z \neq 0$)	0.662811	0.638705	0.609560	0.652890	0.620663
	Zenkour et al. [13] ($\varepsilon z \neq 0$)	0.662811	0.638705	0.609560	0.652890	0.620663
	Zenkour et al. [13] ($\varepsilon z = 0$)	0.688803	0.661291	0.629533	0.677321	0.640940
	TSDT ($\varepsilon z = 0$)	0.688795	0.661260	0.629487	0.677303	0.640905
	Present($\varepsilon z \neq 0$)	0.662751	0.638674	0.609573	0.652833	0.620653
5	Houri et al. [39] ($\varepsilon z \neq 0$)	0.665096	0.642948	0.613842	0.656490	0.624629
	Zenkour et al. [13] ($\varepsilon z \neq 0$)	0.665096	0.642948	0.613842	0.656490	0.624629
	Zenkour et al. [13] ($\varepsilon z = 0$)	0.691420	0.665898	0.634003	0.681343	0.645070
	TSDT ($\varepsilon z = 0$)	0.691415	0.665869	0.633958	0.681327	0.645036
	Present($\varepsilon z \neq 0$)	0.665035	0.642909	0.613851	0.656425	0.624615

Table 9
Comparison of non-dimensional deflection $\bar{w}$of FG sandwich rectangular plates B-type ($p = 3$, $a/h = 10$, $\hat{T}_1 = \hat{T}_3 = 0, \hat{T}_2 = 100$).

Scheme	Theory	$\bar{w}$				
		$a/b = 1$	$a/b = 2$	$a/b = 3$	$a/b = 4$	$a/b = 5$
1-0-1	Houri et al. [39] ($\varepsilon z \neq 0$)	0.658153	0.270902	0.141810	0.088642	0.062334
	Zenkour et al. [13] ($\varepsilon z \neq 0$)	0.658153	0.270902	0.141810	0.088642	0.062334
	Zenkour et al. [13] ($\varepsilon z = 0$)	0.683572	0.273492	0.136798	0.080512	0.052678
	TSDT ($\varepsilon z = 0$)	0.683560	0.273480	0.136786	0.080501	0.052667
	Present($\varepsilon z \neq 0$)	0.658099	0.270846	0.141751	0.088579	0.062266
1-1-1	Houri et al. [39] ($\varepsilon z \neq 0$)	0.631600	0.259980	0.136105	0.085094	0.059862
	Zenkour et al. [13] ($\varepsilon z \neq 0$)	0.631600	0.259980	0.136105	0.085094	0.059862
	Zenkour et al. [13] ($\varepsilon z = 0$)	0.653671	0.261647	0.130971	0.077163	0.050554
	TSDT ($\varepsilon z = 0$)	0.653638	0.261614	0.130939	0.077131	0.050522
	Present($\varepsilon z \neq 0$)	0.631579	0.259958	0.136081	0.085067	0.059830
1-2-1	Houri et al. [39] ($\varepsilon z \neq 0$)	0.602744	0.248135	0.129933	0.081262	0.057192
	Zenkour et al. [13] ($\varepsilon z \neq 0$)	0.602744	0.248135	0.129933	0.081262	0.057192
	Zenkour et al. [13] ($\varepsilon z = 0$)	0.622467	0.249245	0.124837	0.073610	0.048277
	TSDT ($\varepsilon z = 0$)	0.622420	0.249199	0.124791	0.073564	0.048231
	Present($\varepsilon z \neq 0$)	0.602760	0.248150	0.129947	0.081273	0.057199
2-1-2	Houri et al. [39] ($\varepsilon z \neq 0$)	0.646475	0.266094	0.139295	0.087077	0.061244
	Zenkour et al. [13] ($\varepsilon z \neq 0$)	0.646475	0.266094	0.139295	0.087077	0.061244
	Zenkour et al. [13] ($\varepsilon z = 0$)	0.670275	0.268228	0.134212	0.079029	0.051740
	TSDT ($\varepsilon z = 0$)	0.670253	0.268206	0.134190	0.079007	0.051718
	Present($\varepsilon z \neq 0$)	0.646428	0.266046	0.139245	0.087023	0.061185
2-2-1	Houri et al. [39] ($\varepsilon z \neq 0$)	0.614121	0.252758	0.132303	0.082701	0.058168
	Zenkour et al. [13] ($\varepsilon z \neq 0$)	0.614121	0.252758	0.132303	0.082701	0.058168
	Zenkour et al. [13] ($\varepsilon z = 0$)	0.634175	0.253878	0.127112	0.074914	0.049101
	TSDT ($\varepsilon z = 0$)	0.634139	0.253843	0.127077	0.074879	0.049066
	Present($\varepsilon z \neq 0$)	0.614117	0.252753	0.132296	0.082691	0.058153

Table 10
Comparison of non-dimensional axial stress $\bar{\sigma}_{xx}$ of FG sandwich square plates B-type ($a/h = 10$, $\hat{T}_1 = \hat{T}_3 = 0, \hat{T}_2 = 100$).

p	Theory	$\bar{\sigma}_{xx}$				
		1-0-1	1-1-1	1-2-1	2-1-2	2-2-1
0	Houri et al. [39] ($\varepsilon z \neq 0$)	−2.286893	−2.286893	−2.286893	−2.286893	−2.286893
	Zenkour et al. [13] ($\varepsilon z \neq 0$)	−2.286893	−2.286893	−2.286893	−2.286893	−2.286893
	Zenkour et al. [13] ($\varepsilon z = 0$)	−2.079675	−2.079675	−2.079675	−2.079675	−2.079675
	TSDT ($\varepsilon z = 0$)	−2.079675	−2.079675	−2.079675	−2.079675	−2.079675
	Present($\varepsilon z \neq 0$)	−2.286222	−2.286222	−2.286222	−2.286222	−2.286222
1	Houri et al. [39] ($\varepsilon z \neq 0$)	−2.277311	−2.482321	−2.639491	−2.383671	−2.653105
	Zenkour et al. [13] ($\varepsilon z \neq 0$)	−2.277311	−2.482321	−2.639491	−2.383671	−2.653105
	Zenkour et al. [13] ($\varepsilon z = 0$)	−1.993885	−2.144369	−2.261939	−0.071622	−2.276155
	TSDT ($\varepsilon z = 0$)	−1.993921	−2.144422	−2.262000	−2.071668	−2.276209
	Present($\varepsilon z \neq 0$)	−2.276742	−2.481734	−2.638904	−2.383093	−2.652525
2	Houri et al. [39] ($\varepsilon z \neq 0$)	−2.047272	−2.268798	−2.465763	−2.154066	−2.492766
	Zenkour et al. [13] ($\varepsilon z \neq 0$)	−2.047272	−2.268798	−2.465763	−2.154066	−2.492766
	Zenkour et al. [13] ($\varepsilon z = 0$)	−1.824065	−1.982233	−2.127124	−1.899672	−2.152815
	TSDT ($\varepsilon z = 0$)	−1.824089	−1.982285	−2.127193	−1.899711	−2.152872
	Present($\varepsilon z \neq 0$)	−2.046711	−2.268188	−2.465132	−2.153483	−2.492151
3	Houri et al. [39] ($\varepsilon z \neq 0$)	−1.963621	−2.173723	−2.384720	−2.058212	−2.421808
	Zenkour et al. [13] ($\varepsilon z \neq 0$)	−1.963621	−2.173723	−2.384720	−2.058212	−2.421808
	Zenkour et al. [13] ($\varepsilon z = 0$)	−1.764689	−1.911970	−2.065398	−1.830216	−2.099241
	TSDT ($\varepsilon z = 0$)	−1.764705	−1.912017	−2.065467	−1.830246	−2.099296
	Present($\varepsilon z \neq 0$)	−1.963079	−2.173117	−2.384077	−2.057645	−2.421185
4	Houri et al. [39] ($\varepsilon z \neq 0$)	−1.926265	−2.122027	−2.338550	−2.009198	−2.383070
	Zenkour et al. [13] ($\varepsilon z \neq 0$)	−1.926265	−2.122027	−2.338550	−2.009198	−2.383070
	Zenkour et al. [13] ($\varepsilon z = 0$)	−1.738915	−1.874521	−2.030732	−1.795543	−2.070371
	TSDT ($\varepsilon z = 0$)	−1.738925	−1.874564	−2.030800	−1.795568	−2.070424
	Present($\varepsilon z \neq 0$)	−1.925736	−2.121431	−2.337904	−2.008641	−2.382442
5	Houri et al. [39] ($\varepsilon z \neq 0$)	−1.907167	−2.090296	−2.309021	−1.980712	−2.359110
	Zenkour et al. [13] ($\varepsilon z \neq 0$)	−1.907167	−2.090296	−2.309021	−1.980712	−2.359110
	Zenkour et al. [13] ($\varepsilon z = 0$)	−1.726003	−1.851867	−2.008794	−1.775738	−2.052671
	TSDT ($\varepsilon z = 0$)	−1.726010	−1.851906	−2.008861	−1.775759	−2.052722
	Present($\varepsilon z \neq 0$)	−1.906639	−2.089707	−2.308375	−1.980171	−2.358484

proposed by Zenkour and Alghamdi [13] and Houari et al. [39]. From this table can be said that the present results show excellent agreement with other HSDTs with thickness stretching effect [13,39]. From Table 8 can be noticed the influence of the thickness stretching effect, i.e. all the results are below the classical HSDTs without thickness stretching effect. The non-dimensional

Table 11
Comparison of non-dimensional shear stress $\bar{\tau}_{xz}$ of FG sandwich square plates B-type ($a/h = 10$, $\hat{T}_1 = 0, \hat{T}_2 = 100, \hat{T}_3 = -100$, $\Psi(z) = (h/\pi)\sin(\pi z/h)$).

p	Theory	$\bar{\tau}_{xz}$				
		1-0-1	1-1-1	1-2-1	2-1-2	2-2-1
0	SSDT ($\varepsilon z = 0$)	0.574063	0.574063	0.574063	0.574063	0.574063
	TSDT ($\varepsilon z = 0$)	0.500755	0.500754	0.500756	0.500755	0.500755
	ESDT ($\varepsilon z = 0$)	0.652973	0.652968	0.652974	0.652974	0.652974
	Present($\varepsilon z \neq 0$)	0.935581	0.935575	0.935582	0.935581	0.935582
1	SSDT ($\varepsilon z = 0$)	0.696774	0.694817	0.705270	0.689077	0.697901
	TSDT ($\varepsilon z = 0$)	0.610819	0.608191	0.616563	0.603833	0.610784
	ESDT ($\varepsilon z = 0$)	0.788591	0.787704	0.800620	0.780259	0.791324
	Present($\varepsilon z \neq 0$)	1.113178	1.104483	1.118084	1.097516	1.108004
2	SSDT ($\varepsilon z = 0$)	0.696044	0.689620	0.711266	0.679194	0.699571
	TSDT ($\varepsilon z = 0$)	0.611291	0.604406	0.621976	0.596351	0.612794
	ESDT ($\varepsilon z = 0$)	0.786235	0.780821	0.807255	0.767484	0.792494
	Present($\varepsilon z \neq 0$)	1.116100	1.097021	1.126337	1.083845	1.110129
3	SSDT ($\varepsilon z = 0$)	0.697635	0.681516	0.710627	0.669256	0.696850
	TSDT ($\varepsilon z = 0$)	0.613193	0.597865	0.621613	0.588429	0.610801
	ESDT ($\varepsilon z = 0$)	0.787282	0.770848	0.806292	0.755146	0.788879
	Present($\varepsilon z \neq 0$)	1.121996	1.085657	1.125663	1.070193	1.106545
4	SSDT ($\varepsilon z = 0$)	0.702617	0.674664	0.708782	0.662291	0.694226
	TSDT ($\varepsilon z = 0$)	0.617736	0.592304	0.620163	0.582918	0.608798
	ESDT ($\varepsilon z = 0$)	0.792637	0.762536	0.803995	0.746567	0.785561
	Present($\varepsilon z \neq 0$)	1.132314	1.076034	1.123274	1.060707	1.103159
5	SSDT ($\varepsilon z = 0$)	0.709315	0.669326	0.706821	0.657748	0.692220
	TSDT ($\varepsilon z = 0$)	0.623594	0.587945	0.618581	0.579263	0.607206
	ESDT ($\varepsilon z = 0$)	0.800201	0.756055	0.801603	0.740835	0.782997
	Present($\varepsilon z \neq 0$)	1.144742	1.068461	1.120660	1.054447	1.100541

Table 12
Comparison of non-dimensional shear stress $\bar{\tau}_{xz}$ of FG sandwich square plates B-type ($a/h = 10$, $\hat{T}_1 = 0, \hat{T}_2 = 100, \hat{T}_3 = -100$, $\Psi(z) = z(1 - (4/3)(z/h)^2)$).

p	Theory	$\bar{\tau}_{xz}$				
		1-0-1	1-1-1	1-2-1	2-1-2	2-2-1
0	SSDT ($\varepsilon z = 0$)	0.534052	0.534051	0.534053	0.534052	0.534052
	TSDT ($\varepsilon z = 0$)	0.466349	0.466349	0.466349	0.466349	0.466349
	ESDT ($\varepsilon z = 0$)	0.606835	0.606843	0.606847	0.606847	0.606847
	Present($\varepsilon z \neq 0$)	0.863015	0.863017	0.863022	0.863014	0.863018
1	SSDT ($\varepsilon z = 0$)	0.642807	0.639130	0.647939	0.634648	0.641868
	TSDT ($\varepsilon z = 0$)	0.564059	0.559957	0.566925	0.556662	0.562231
	ESDT ($\varepsilon z = 0$)	0.726840	0.723949	0.734947	0.717989	0.727194
	Present($\varepsilon z \neq 0$)	1.019997	1.009700	1.021192	1.004311	1.012863
2	SSDT ($\varepsilon z = 0$)	0.643680	0.634641	0.653016	0.626415	0.643355
	TSDT ($\varepsilon z = 0$)	0.565881	0.556769	0.571546	0.550567	0.564062
	ESDT ($\varepsilon z = 0$)	0.726352	0.717903	0.740512	0.707159	0.728181
	Present($\varepsilon z \neq 0$)	1.024605	1.003182	1.028106	0.992852	1.014690
3	SSDT ($\varepsilon z = 0$)	0.646333	0.627679	0.652527	0.618097	0.641156
	TSDT ($\varepsilon z = 0$)	0.568711	0.551237	0.571319	0.544027	0.562514
	ESDT ($\varepsilon z = 0$)	0.728634	0.709285	0.739720	0.696719	0.725184
	Present($\varepsilon z \neq 0$)	1.031528	0.993430	1.027607	0.981414	1.011794
4	SSDT ($\varepsilon z = 0$)	0.651739	0.621793	0.650969	0.612345	0.639036
	TSDT ($\varepsilon z = 0$)	0.573625	0.546463	0.570117	0.539446	0.560893
	ESDT ($\varepsilon z = 0$)	0.734471	0.702079	0.737753	0.689496	0.722427
	Present($\varepsilon z \neq 0$)	1.042022	0.985132	1.025595	0.973508	1.009040
5	SSDT ($\varepsilon z = 0$)	0.658483	0.617183	0.649285	0.608552	0.637373
	TSDT ($\varepsilon z = 0$)	0.579530	0.542724	0.568771	0.536526	0.559642
	ESDT ($\varepsilon z = 0$)	0.742073	0.696448	0.735680	0.684707	0.720296
	Present($\varepsilon z \neq 0$)	1.054138	0.978585	1.023354	0.968338	1.006908

deflection increases as the exponent increases. Because this pattern holds for both types of sandwich plates with different schemes, it can be said that this behavior holds true for general FG sandwich plates.

Table 9 presents results of non-dimensional deflections $\bar{w}$ of FG sandwich plates for different values of aspect ratio "a/b" and several sandwich schemes, considering an exponent $p = 3$. As before, the sandwich plate is subjected to a linear temperature distribution through the thickness ($\hat{T}_3 = 0$). The results are compared with several HSDTs as in Table 8. The results of the present theory show excellent agreement with other theories with thickness stretching effect, as expected. Again, it can be seen that the aspect ratio "a/b" is more influential on the deflection than the exponent "p". For the same sandwich scheme, the sandwich plate B-type has higher deflection than the sandwich plate A-type except for the exponent $p = 0$ (see Tables 4, 5, 8 and 9).

Results of non-dimensional axial stresses $\bar{\sigma}_{xx}$ of FG sandwich square plates for several values of exponent "p" and different

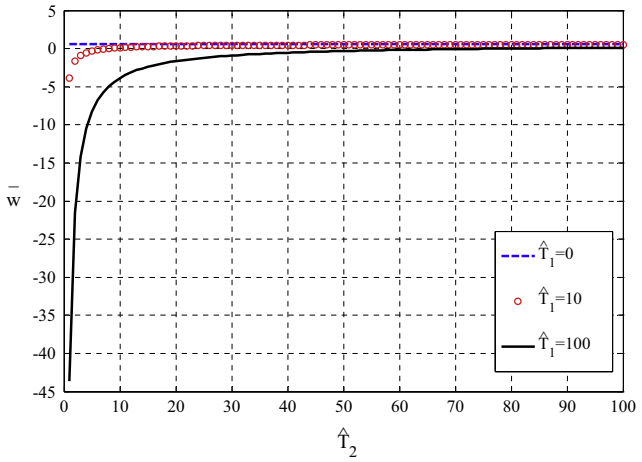

Fig. 5. Variation of non-dimensional deflection $\bar{w}$ of FG sandwich square plate A-type versus the coefficient of the thermal load $\widehat{T}_2$ ($\widehat{T}_3 = 0$, $a/h = 10$, $p = 2$, 1-1-1).

sandwich schemes are presented in Table 10. The sandwich plate is subjected to a linear temperature distribution through the thickness ($\widehat{T}_3 = 0$). The present results show an excellent agreement with other solutions with stretching effect [13,39]. From this table it can be seen that the non-dimensional axial stress decrease as the exponent "p" increase, except for the exponent $p = 0$. Again, it can be seen that the present results are higher (in absolute value) than the other solutions due to the influence of the thickness stretching effect.

In Tables 11 and 12 the results of the non-dimensional transverse shear stress $\bar{\tau}_{xz}$ of FG sandwich square plates considering a generalized temperature field are presented. The results of this theory are compared with solutions based on HSDTs proposed by Reddy [43], Touratier [44] and Karama [45,46] which were reproduced in this paper for the present analysis. Table 11 presents results of non-dimensional transverse shear stress considering a sine function in the nonlinear temperature distribution, i.e., $\Psi(z) = (h/\pi)\ \sin(\pi z/h)$; and Table 12 considering a polynomial function in the nonlinear temperature distribution, i.e., $\Psi(z) = z(1 - (4/3)(z/h)^2)$. From these tables can be noticed that the present results are higher than the other solutions in all cases. It is worth highlighting that nonlinear temperature field with polynomial function produces lower values of transverse shear stress, see Tables 11 and 12. The non-dimensional transverse shear stresses do not follow a particular pattern with respect to the exponent "p". This fact is also shown in the next section.

4.4. Study of the effect of thermal loads on FG sandwich plates

In this section the variation of non-dimensional deflection, $\bar{w}$, axial stress, $\bar{\sigma}_{xx}$, and transverse shear stress results, $\bar{\tau}_{xz}$, with respect to the thermal loads T_1, T_2 and T_3, for both types of sandwich plates, are presented.

Figs. 5 and 6 show the variation of the non-dimensional deflection $\bar{w}$ and non-dimensional stresses $(\bar{\sigma}_{xx}, \bar{\tau}_{xz})$ as a function of the coefficient of thermal load $\widehat{T}_2$ of FG sandwich square plate A-type for various values of $\widehat{T}_1 = \{0, 10, 100\}$, respectively. Fig. 5 shows the strong influence of temperature coefficient $\widehat{T}_1$ on the non-dimensional deflection. This effect increases for high values of thermal coefficient $\widehat{T}_1$ and low values of coefficient of thermal load $\widehat{T}_2$. Likewise, in Fig. 6 it can be seen that the coefficient of thermal load $\widehat{T}_1$ also influences the results of the non-dimensional axial and transverse shear stresses.

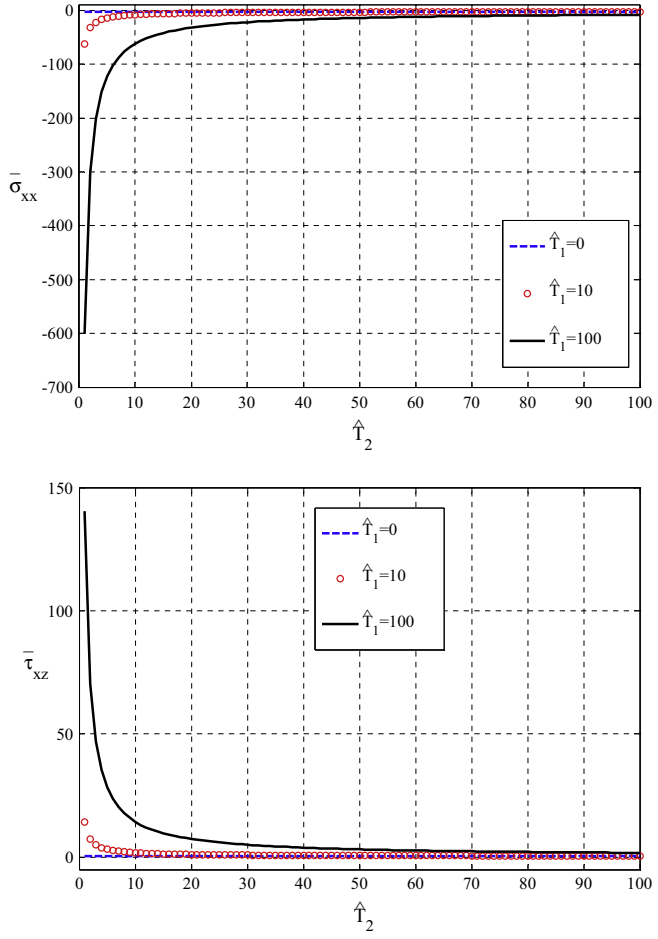

Fig. 6. Variation of non-dimensional stresses $\bar{\sigma}_{xx}$, $\bar{\tau}_{xz}$ of FG sandwich square plate A-type versus the coefficient of the thermal load $\widehat{T}_2(\widehat{T}_3 = 0, a/h = 10, p = 2$, 1-1-1).

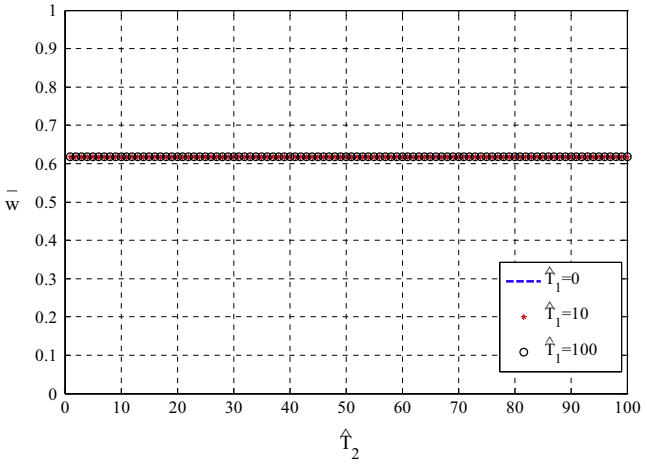

Fig. 7. Variation of non-dimensional deflection $\bar{w}$ of FG sandwich square plate B-type versus the coefficient of the thermal load $\widehat{T}_2(\widehat{T}_3 = 0, a/h = 10, p = 2$, 1-1-1).

Figs. 7 and 8 show the variation of the non-dimensional deflection $\bar{w}$ and non-dimensional stresses $(\bar{\sigma}_{xx}, \bar{\tau}_{xz})$ as a function of the coefficient of thermal load $\widehat{T}_2$ of FG sandwich square plates B-type for various values of $\widehat{T}_1 = \{0, 10, 100\}$, respectively. From these figures can be seen that the coefficient of thermal load $\widehat{T}_1$ does not

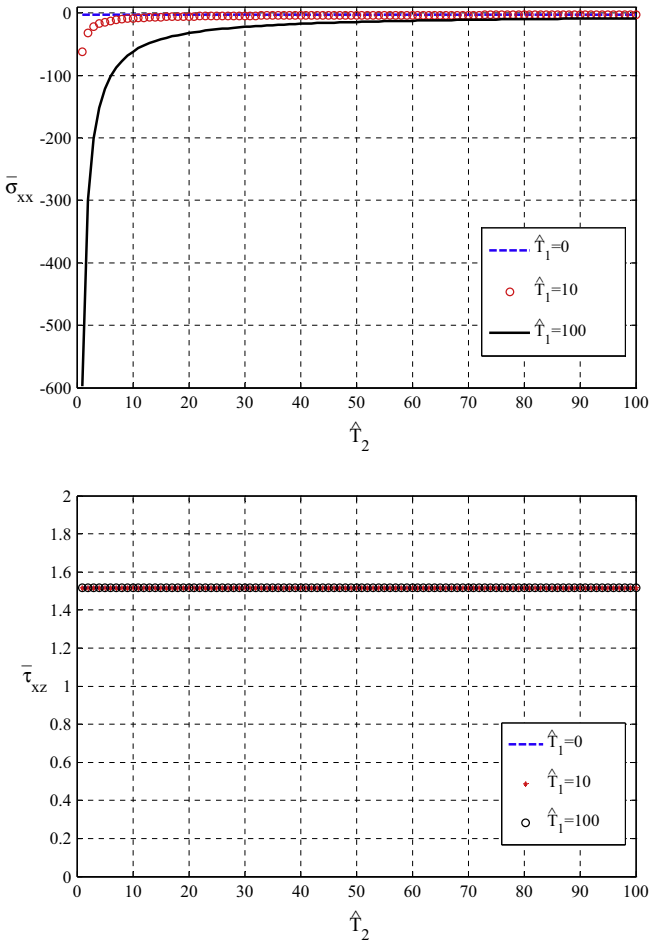

Fig. 8. Variation of non-dimensional stresses $\bar{\sigma}_{xx}$, $\bar{\tau}_{xz}$ of FG sandwich square plate B-type versus the coefficient of the thermal load $\hat{T}_2(\hat{T}_3 = 0, a/h = 10, p = 2$, 1-1-1).

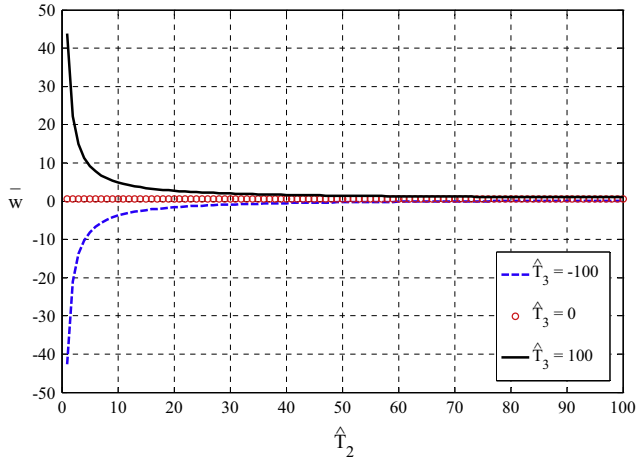

Fig. 9. Variation of non-dimensional deflection $\bar{w}$ of FG sandwich square plate A-type versus the coefficient of the thermal load $\hat{T}_2$ considering a nonlinear temperature field with a sine function $(\Psi(z) = (h/\pi)\sin(\pi z/h), \hat{T}_1 = 0,\ a/h = 10,$ $p = 2$, 1-1-1).

influence the results of the non-dimensional deflections and transverse shear stresses, contrary to what happens for a sandwich plate A-type.

Figs. 9 and 10 show the variation of the non-dimensional deflection $\bar{w}$ and non-dimensional stresses $(\bar{\sigma}_{xx}, \bar{\tau}_{xz})$ as a function of the

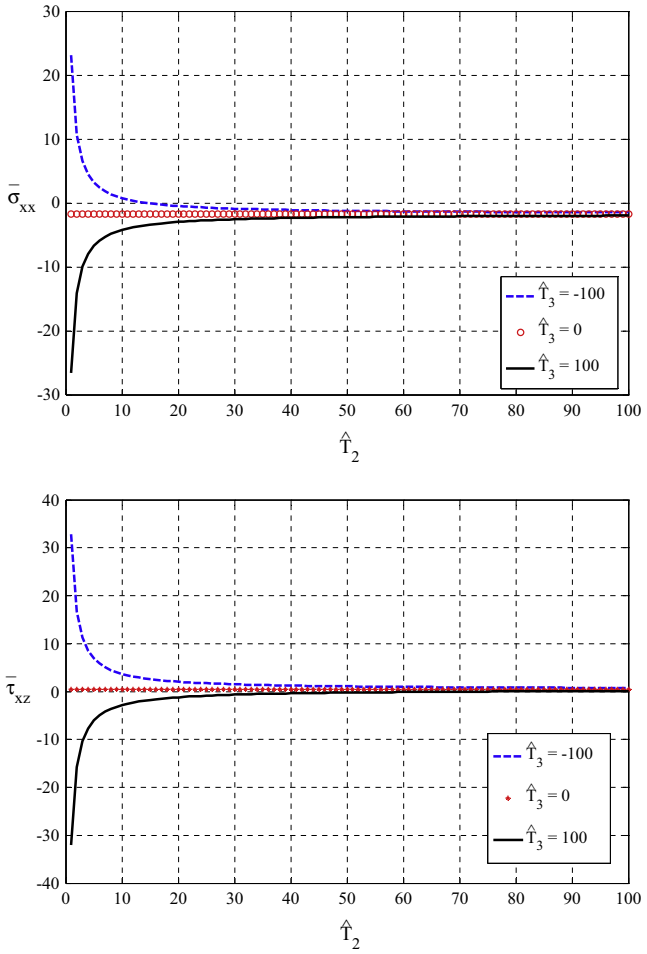

Fig. 10. Variation of non-dimensional stresses $\bar{\sigma}_{xx}$, $\bar{\tau}_{xz}$ of FG sandwich square plate A-type versus the coefficient of the thermal load $\hat{T}_2$ considering a nonlinear temperature field with a sine function $(\Psi(z) = (h/\pi)\sin(\pi z/h), \hat{T}_1 = 0,\ a/h = 10,$ $p = 2$, 1-1-1).

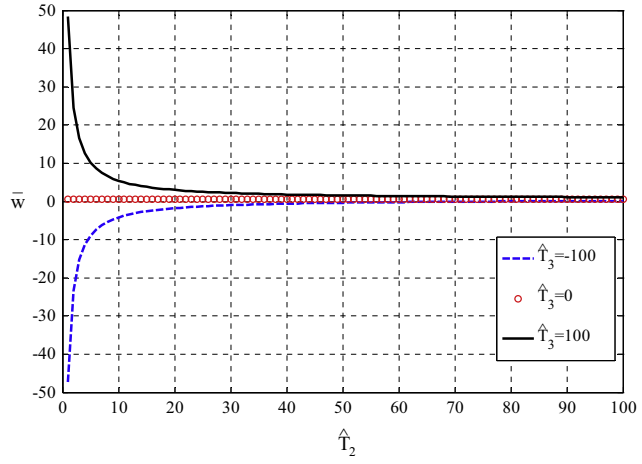

Fig. 11. Variation of non-dimensional deflection $\bar{w}$ of FG sandwich square plate B-type versus the coefficient of the thermal load $\hat{T}_2$ considering a nonlinear temperature field with a sine function $(\Psi(z) = (h/\pi)\sin(\pi z/h), \hat{T}_1 = 0,\ a/h = 10,$ $p = 2$, 1-1-1).

coefficient of thermal load $\hat{T}_2$ of FG sandwich square plate A-type for various values of $\hat{T}_3 = \{-100, 0, 100\}$, respectively. These figures show that the coefficient $\hat{T}_3$ influences the non-dimensional

deflection and non-dimensional axial and transverse shear stress. However, the influence is reduced a lot with the increase of the coefficient of thermal load $\widehat{T}_2$. Similar results to the previous figures were obtained for the sandwich plate B-type and they are shown in Figs. 11 and 12.

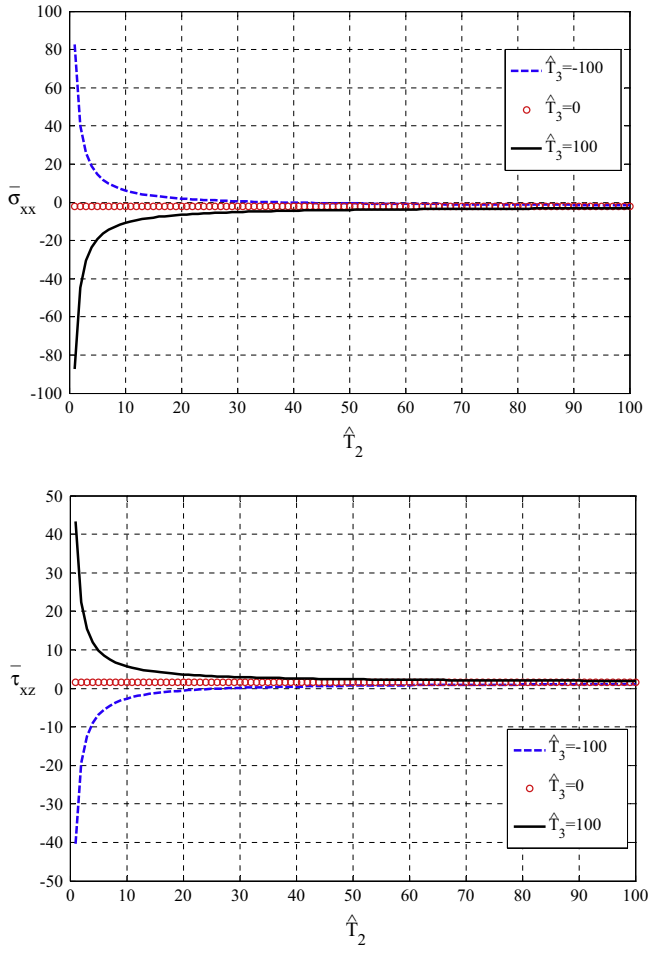

Fig. 12. Variation of non-dimensional stresses $\bar{\sigma}_{xx}$, $\bar{\tau}_{xz}$ of FG sandwich square plate B-type versus the coefficient of the thermal load $\widehat{T}_2$ considering a nonlinear temperature field with a sine function ($\Psi(z) = (h/\pi)\sin(\pi z/h), \widehat{T}_1 = 0$, $a/h = 10$, $p = 2$, 1-1-1).

Figs. 13 and 14 show the distribution of non-dimensional deflection $\bar{w}$ and stresses $(\bar{\sigma}_{xx}, \bar{\tau}_{xz})$ across the thickness direction for FG sandwich plate A-type for several values of the coefficient of thermal load $\widehat{T}_3 = \{-100, 0, 100\}$, respectively. From Fig. 13 can be noted that the non-dimensional deflection increases due

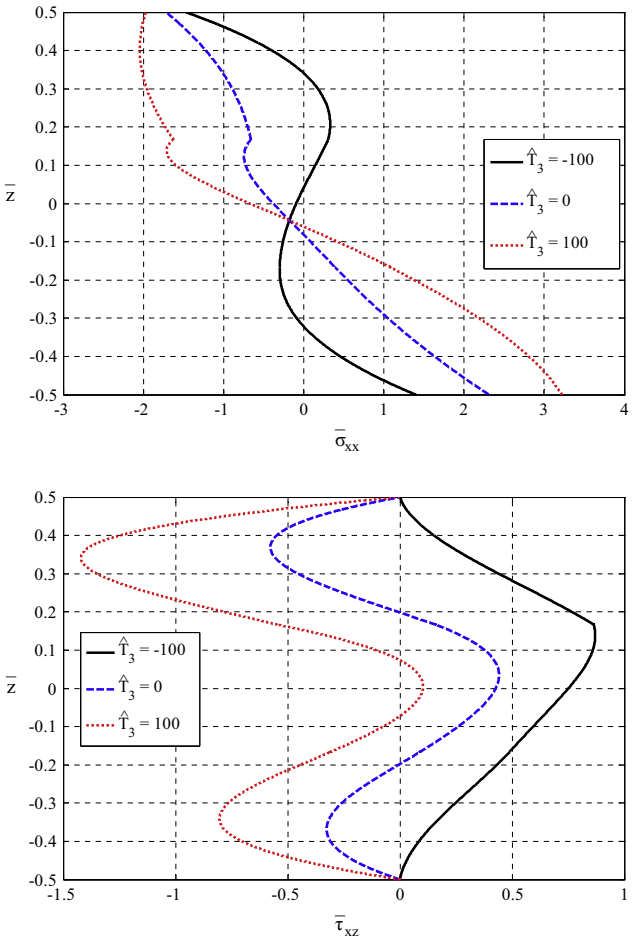

Fig. 14. Distribution of non-dimensional stresses $\bar{\sigma}_{xx}, \bar{\tau}_{xz}$ through the thickness of a FG sandwich square plate A-type considering a nonlinear temperature field with a sine function ($\Psi(z) = (h/\pi)\sin(\pi z/h), \widehat{T}_1 = 0, \widehat{T}_2 = 100$, $a/h = 10$, $p = 2$, 1-1-1).

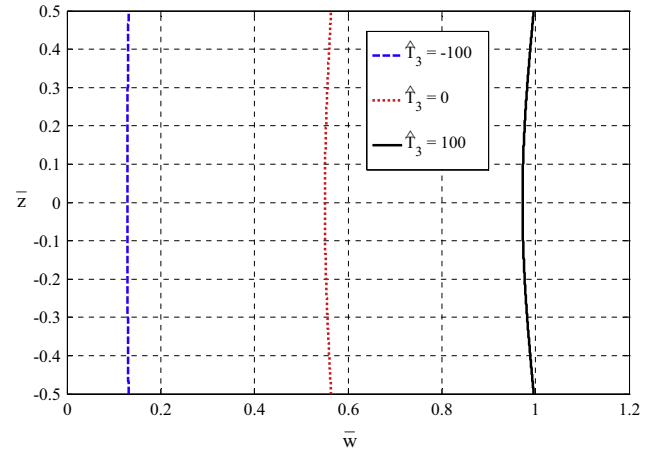

Fig. 13. Distribution of non-dimensional deflection $\bar{w}$ through the thickness of a FG sandwich square plate A-type considering a nonlinear temperature field with a sine function ($\Psi(z) = (h/\pi)\sin(\pi z/h), \widehat{T}_1 = 0, \widehat{T}_2 = 100$, $a/h = 10$, $p = 2$, 1-1-1).

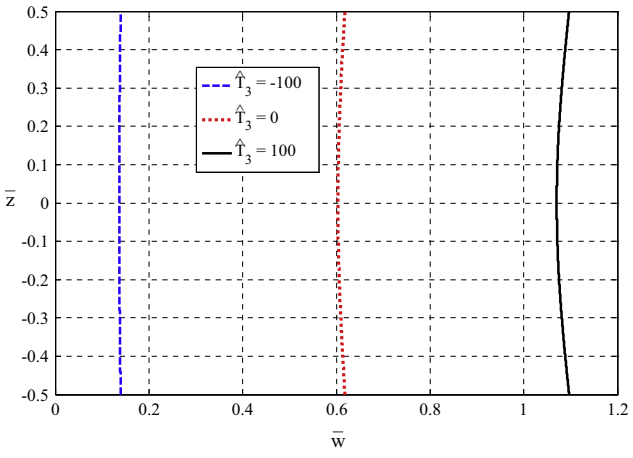

Fig. 15. Distribution of non-dimensional deflection $\bar{w}$ through the thickness of a FG sandwich square plate B-type considering a nonlinear temperature field with a sine function ($\Psi(z) = (h/\pi)\sin(\pi z/h), \widehat{T}_1 = 0, \widehat{T}_2 = 100$, $a/h = 10$, $p = 2$, 1-1-1).

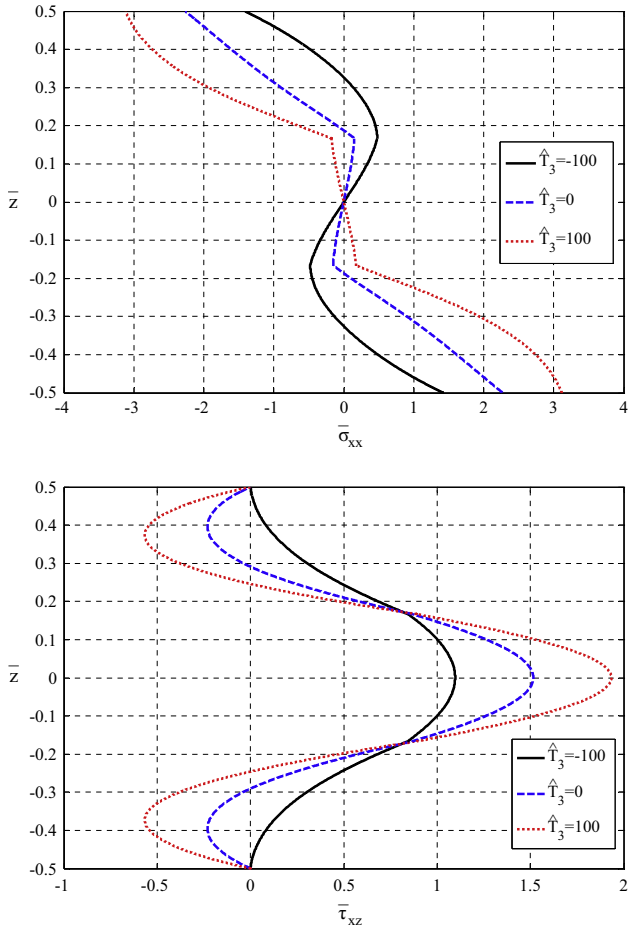

Fig. 16. Distribution of non-dimensional stresses $\bar{\sigma}_{xx}, \bar{\tau}_{xz}$ through the thickness of a FG sandwich square plate B-type considering a nonlinear temperature field with a sine function ($\Psi(z) = (h/\pi)\sin(\pi z/h), \widehat{T}_1 = 0, \widehat{T}_2 = 100$, a/h = 10, p = 2, 1-1-1).

to increase of coefficient $\widehat{T}_3$. Non-dimensional deflection takes its maximum value on the surfaces of the sandwich plate. However, the effect disappears when the coefficient $\widehat{T}_3 = -100$. In Fig. 14 it can be seen that the coefficient of thermal load $\widehat{T}_3$ significantly influences the results of the non-dimensional axial and transverse shear stresses.

Figs. 15 and 16 show the effect of the thermal coefficient $\widehat{T}_3$ on the distribution of the non-dimensional deflection $\bar{w}$ and stresses $(\bar{\sigma}_{xx}, \bar{\tau}_{xz})$, respectively, across the thickness direction for FG sandwich plate B-type. The curves of Fig. 15 have the same tendency as the results of the deflection of a sandwich plate A-type (see Fig. 13). However, in this case, the non-dimensional deflections are higher. Again, it can be noticed that the coefficient of thermal load $\widehat{T}_3$ has a significant influence on the results.

5. Conclusions

This paper presents a thermoelastic bending analysis for two different types of FG sandwich plates with different schemes by using a new quasi-3D hybrid type HSDT subjected to a generalized temperature field. Many hybrid shear deformation theories with only 5 unknowns can be derived by using the present generalized formulation. The nonlinear term of the temperature field can be different from the shear strain shape functions of the displacement field. The governing equations are obtained through the principle of virtual works. These equations are solved via Navier's method. The results were compared with the solutions of several theories. It is concluded that the results of the present theory has an excellent agreement with other theories with thickness stretching effect for the thermoelastic static problem. The non-dimensional stresses $\bar{\sigma}_{xx}, \bar{\tau}_{xz}$ and non-dimensional deflection $\bar{w}$ are sensitive to the nonlinear term of the temperature field. The nature of the nonlinear term of the temperature field strongly affects the results.

Acknowledgment

This work has been performed due to the opportunity, confidence and special support of the following Persons: Carlos Heeren, Alberto Bejarano, Enrique Sarmiento and Alexander Peralta.

Appendix A. Definition of constants in Eq. (29)

As mentioned before, these matrices are associated with the expressions of the plate governing Eq. (19a-e) they used to calculate the K_{ij} element matrices. The advantage of the present technique is that infinite shear deformation theories can be created and calculated by using the same following matrices, only "y^* and q^*" should be changed.

$$\overline{M}^{0,0} = \begin{bmatrix} -\lambda & 0 & 0 & 0 & 0 \\ 0 & -\beta & 0 & 0 & 0 \\ 0 & 0 & 0 & 0 & 0 \\ 0 & 0 & y^*\beta & 0 & q^*\beta \\ 0 & 0 & y^*\lambda & 0 & q^*\lambda \\ \beta & \lambda & 0 & 0 & 0 \end{bmatrix}, \quad \overline{M}^{0,1} = \begin{bmatrix} 0 & 0 & -y^{**}\lambda^2 & \lambda^2 & -q^*\lambda^2 \\ 0 & 0 & -y^{**}\beta^2 & \beta^2 & -q^*\beta^2 \\ 0 & 0 & 0 & 0 & 0 \\ 0 & 0 & 0 & 0 & 0 \\ 0 & 0 & 0 & 0 & 0 \\ 0 & 0 & 2y^{**}\lambda\beta & -2\lambda\beta & 2q^*\lambda\beta \end{bmatrix}$$

$$\overline{M}^{0,2} = \begin{bmatrix} 0 & 0 & -\lambda^2 & 0 & 0 \\ 0 & 0 & -\beta^2 & 0 & 0 \\ 0 & 0 & 0 & 0 & 0 \\ 0 & 0 & 0 & 0 & 0 \\ 0 & 0 & 0 & 0 & 0 \\ 0 & 0 & 2\lambda\beta & 0 & 0 \end{bmatrix}, \quad \overline{M}^{0,3} = \begin{bmatrix} 0 & 0 & 0 & 0 & 0 \\ 0 & 0 & 0 & 0 & 0 \\ 0 & 0 & 0 & 0 & 0 \\ 0 & 0 & 0 & 0 & \beta \\ 0 & 0 & 0 & 0 & \lambda \\ 0 & 0 & 0 & 0 & 0 \end{bmatrix}$$

$$\overline{M}^{0,4} = \begin{bmatrix} 0 & 0 & 0 & 0 & 0 \\ 0 & 0 & 0 & 0 & 0 \\ 0 & 0 & 0 & 0 & 0 \\ 0 & 0 & \beta & 0 & 0 \\ 0 & 0 & \lambda & 0 & 0 \\ 0 & 0 & 0 & 0 & 0 \end{bmatrix}, \quad \overline{M}^{0,5} = \begin{bmatrix} 0 & 0 & 0 & 0 & 0 \\ 0 & 0 & 0 & 0 & 0 \\ 0 & 0 & 0 & 0 & 1 \\ 0 & 0 & 0 & 0 & 0 \\ 0 & 0 & 0 & 0 & 0 \\ 0 & 0 & 0 & 0 & 0 \end{bmatrix}$$

$$\overline{M}_x^{1,0} = \begin{bmatrix} -\lambda^2 & 0 & 0 & 0 & 0 \\ 0 & -\lambda\beta & 0 & 0 & 0 \\ 0 & 0 & 0 & 0 & 0 \\ 0 & 0 & y^*\lambda\beta & 0 & q^*\lambda\beta \\ 0 & 0 & -y^*\lambda^2 & 0 & -q^*\lambda^2 \\ -\lambda\beta & -\lambda^2 & 0 & 0 & 0 \end{bmatrix}$$

$$\overline{M}_x^{1,1} = \begin{bmatrix} 0 & 0 & -y^{**}\lambda^3 & \lambda^3 & -q^*\lambda^3 \\ 0 & 0 & -y^{**}\lambda\beta^2 & \lambda\beta^2 & -q^*\lambda\beta^2 \\ 0 & 0 & 0 & 0 & 0 \\ 0 & 0 & 0 & 0 & 0 \\ 0 & 0 & 0 & 0 & 0 \\ 0 & 0 & -2y^{**}\lambda^2\beta & 2\lambda^2\beta & -2q^*\lambda^2\beta \end{bmatrix}$$

$$\overline{M}_x^{1,2}=\begin{bmatrix}0&0&-\lambda^3&0&0\\0&0&-\lambda\beta^2&0&0\\0&0&0&0&0\\0&0&0&0&0\\0&0&0&0&0\\0&0&-2\lambda^2\beta&0&0\end{bmatrix},\quad \overline{M}_x^{1,3}=\begin{bmatrix}0&0&0&0&0\\0&0&0&0&0\\0&0&0&0&0\\0&0&0&0&\lambda\beta\\0&0&0&0&-\lambda^2\\0&0&0&0&0\end{bmatrix}$$

$$\overline{M}_x^{1,4}=\begin{bmatrix}0&0&0&0&0\\0&0&0&0&0\\0&0&0&0&0\\0&0&\lambda\beta&0&0\\0&0&-\lambda^2&0&0\\0&0&0&0&0\end{bmatrix},\quad \overline{M}_x^{1,5}=\begin{bmatrix}0&0&0&0&0\\0&0&0&0&0\\0&0&0&0&\lambda\\0&0&0&0&0\\0&0&0&0&0\\0&0&0&0&0\end{bmatrix}$$

$$\overline{M}_y^{1,0}=\begin{bmatrix}-\lambda\beta&0&0&0&0\\0&-\beta^2&0&0&0\\0&0&0&0&0\\0&0&-y^*\beta^2&0&-q^*\beta^2\\0&0&y^*\lambda\beta&0&q^*\lambda\beta\\-\beta^2&-\lambda\beta&0&0&0\end{bmatrix},$$

$$\overline{M}_y^{1,1}=\begin{bmatrix}0&0&-y^{**}\lambda^2\beta&\lambda^2\beta&-q^*\lambda^2\beta\\0&0&-y^{**}\beta^3&\beta^3&-q^*\beta^3\\0&0&0&0&0\\0&0&0&0&0\\0&0&0&0&0\\0&0&-2y^{**}\lambda\beta^2&2\lambda\beta^2&-2q^*\lambda\beta^2\end{bmatrix}$$

$$\overline{M}_y^{1,2}=\begin{bmatrix}0&0&-\lambda^2\beta&0&0\\0&0&-\beta^3&0&0\\0&0&0&0&0\\0&0&0&0&0\\0&0&0&0&0\\0&0&-2\lambda\beta^2&0&0\end{bmatrix},\quad \overline{M}_y^{1,3}=\begin{bmatrix}0&0&0&0&0\\0&0&0&0&0\\0&0&0&0&0\\0&0&0&0&-\beta^2\\0&0&0&0&\lambda\beta\\0&0&0&0&0\end{bmatrix}$$

$$\overline{M}_y^{1,4}=\begin{bmatrix}0&0&0&0&0\\0&0&0&0&0\\0&0&0&0&0\\0&0&-\beta^2&0&0\\0&0&\lambda\beta&0&0\\0&0&0&0&0\end{bmatrix},\quad \overline{M}_y^{1,5}=\begin{bmatrix}0&0&0&0&0\\0&0&0&0&0\\0&0&0&0&\beta\\0&0&0&0&0\\0&0&0&0&0\\0&0&0&0&0\end{bmatrix}$$

$$\overline{M}_y^{2,0}=\begin{bmatrix}\lambda\beta^2&0&0&0&0\\0&\beta^3&0&0&0\\0&0&0&0&0\\0&0&-y^*\beta^3&0&-q^*\beta^3\\0&0&-y^*\lambda\beta^2&0&-q^*\lambda\beta^2\\-\beta^3&-\lambda\beta^2&0&0&0\end{bmatrix}$$

$$\overline{M}_y^{2,1}=\begin{bmatrix}0&0&y^{**}\lambda^2\beta^2&-\lambda^2\beta^2&q^*\lambda^2\beta^2\\0&0&y^{**}\beta^4&-\beta^4&q^*\beta^4\\0&0&0&0&0\\0&0&0&0&0\\0&0&0&0&0\\0&0&-2y^{**}\lambda\beta^3&2\lambda\beta^3&-2q^*\lambda\beta^3\end{bmatrix}$$

$$\overline{M}_y^{2,2}=\begin{bmatrix}0&0&\lambda^2\beta^2&0&0\\0&0&\beta^4&0&0\\0&0&0&0&0\\0&0&0&0&0\\0&0&0&0&0\\0&0&-2\lambda\beta^3&0&0\end{bmatrix},\quad \overline{M}_y^{2,3}=\begin{bmatrix}0&0&0&0&0\\0&0&0&0&0\\0&0&0&0&0\\0&0&0&0&-\beta^3\\0&0&0&0&-\lambda\beta^2\\0&0&0&0&0\end{bmatrix}$$

$$\overline{M}_y^{2,4}=\begin{bmatrix}0&0&0&0&0\\0&0&0&0&0\\0&0&0&0&0\\0&0&-\beta^3&0&0\\0&0&-\lambda\beta^2&0&0\\0&0&0&0&0\end{bmatrix},\quad \overline{M}_y^{2,5}=\begin{bmatrix}0&0&0&0&0\\0&0&0&0&0\\0&0&0&0&-\beta^2\\0&0&0&0&0\\0&0&0&0&0\\0&0&0&0&0\end{bmatrix}$$

$$\overline{M}_{xy}^{2,0}=\begin{bmatrix}-\lambda^2\beta&0&0&0&0\\0&-\lambda\beta^2&0&0&0\\0&0&0&0&0\\0&0&-y^*\lambda\beta^2&0&-q^*\lambda\beta^2\\0&0&-y^*\lambda^2\beta&0&-q^*\lambda^2\beta\\\lambda\beta^2&\lambda^2\beta&0&0&0\end{bmatrix}$$

$$\overline{M}_{xy}^{2,1}=\begin{bmatrix}0&0&-y^{**}\lambda^3\beta&\lambda^3\beta&-q^*\lambda^3\beta\\0&0&-y^{**}\lambda\beta^3&\lambda\beta^3&-q^*\lambda\beta^3\\0&0&0&0&0\\0&0&0&0&0\\0&0&0&0&0\\0&0&2y^{**}\lambda^2\beta^2&-2\lambda^2\beta^2&2q^*\lambda^2\beta^2\end{bmatrix}$$

$$\overline{M}_{xy}^{2,2}=\begin{bmatrix}0&0&-\lambda^3\beta&0&0\\0&0&-\lambda\beta^3&0&0\\0&0&0&0&0\\0&0&0&0&0\\0&0&0&0&0\\0&0&2\lambda^2\beta^2&0&0\end{bmatrix},\quad \overline{M}_{xy}^{2,3}=\begin{bmatrix}0&0&0&0&0\\0&0&0&0&0\\0&0&0&0&0\\0&0&0&0&-\lambda\beta^2\\0&0&0&0&-\lambda^2\beta\\0&0&0&0&0\end{bmatrix}$$

$$\overline{M}_{xy}^{2,4}=\begin{bmatrix}0&0&0&0&0\\0&0&0&0&0\\0&0&0&0&0\\0&0&-\lambda\beta^2&0&0\\0&0&-\lambda^2\beta&0&0\\0&0&0&0&0\end{bmatrix},\quad \overline{M}_{xy}^{2,5}=\begin{bmatrix}0&0&0&0&0\\0&0&0&0&0\\0&0&0&0&\lambda\beta\\0&0&0&0&0\\0&0&0&0&0\\0&0&0&0&0\end{bmatrix}$$

References

[1] Chamis CC. Probabilistic design of composite structures. ICCES 2007;4(2):59–66.
[2] Allen HG. Analysis and design of structural sandwich plates. Oxford: Pergamon Press; 1969.
[3] Larsson L, Eliasson R. Principles of yacht design. Great Britain: International Marine (A division of the McGraw-Hill Companies); 2000.
[4] Mouritz AP, Gellert E, Burchill P, Challis K. Review of advanced composite structures for naval ships and submarines. Compos Struct 2001;53:21–41.
[5] Russo A, Zuccarello B. Experimental and numerical evaluation of the mechanical behavior of GFRP sandwich plates. Compos Struct 2007;81:575–86.
[6] Vinson JR. The behavior of sandwich structures of isotropic and composite materials. Lancaster (PA, USA): THECHNOMIC Publishing Company Inc.; 1999.
[7] Vinson JR. Sandwich structures. Appl Mech Rev 2001;54(3):201–14.
[8] Vinson JR. Sandwich structures: past, present, and future. In: Proceedings of the 7th international conference on sandwich structures. Aalborg, Denmark: Aalborg University; 2005. p. 3–12. 29–31 August.

[9] Polit O, Touratier M. High-order triangular sandwich plate finite element for linear and non-linear analyses. Comput Methods Appl Mech Eng 2000;185:305–24.
[10] Kant T, Swaminathan K. Analytical solutions for the static analysis of laminated composite and sandwich plates based on a higher order refined theory. Compos Struct 2002;56:329–44.
[11] Matsunaga H. A comparison between 2-D single-layer and 3-D layerwise theories for computing interlaminar stresses of laminated composite and sandwich plates subjected to thermal loadings. Compos Struct 2004;64:161–77.
[12] Ferreira AJM, Roque CMC, Jorge RMN, Kansa EJ. Static deformations and vibration analysis of composite and sandwich plates using a layerwise theory and multiquadrics discretizations. Eng Anal Bound Elem 2005;29:1104–14.
[13] Zenkour AM, Alghamdi NA. Thermoelastic bending analysis of functionally graded sandwich plates. J Mater Sci 2008;43:2574–89.
[14] Xiang S, Wang K, Ai Y, Sha Y, Shi H. Analysis of isotropic, sandwich and laminated plates by a meshless method and various shear deformation theories. Compos Struct 2009;91:31–7.
[15] Cetkovic M, Vuksanovic Dj. Bending, free vibrations and buckling of laminated composite and sandwich plates using a layerwise displacement model. Compos Struct 2000;88:219–27.
[16] Shariyat M. A generalized high-order global–local plate theory for nonlinear bending and buckling analyses of imperfect sandwich plates subjected to thermo-mechanical loads. Compos Struct 2010;92:130–43.
[17] Shariyat M. A generalized high-order global-local plate theory for nonlinear bending and buckling analyses of imperfect sandwich plates subjected to thermo-mechanical loads. Compos Struct 2010;92:130–43.
[18] Zenkour AM, Sobhy M. Thermal buckling of various types of FGM sandwich plates. Compos Struct 2010;93:93–102.
[19] Mantari JL, Oktem AS, Guedes Soares C. Static and dynamic analysis of laminated composite and sandwich plates and shells by using a new higher-order shear deformation theory. Compos Struct 2011;94:37–49.
[20] Mantari JL, Oktem AS, Guedes Soares C. A new trigonometric shear deformation theory for isotropic, laminated composite and sandwich plates. Int J Solids Struct 2012;49:43–53.
[21] Mantari JL, Oktem AS, Guedes Soares C. A new higher order shear deformation theory for sandwich and composite laminated plates. Composites: Part B 2012;43(3):1489–99.
[22] Mantari JL, Oktem AS, Guedes Soares C. A new trigonometric layerwise shear deformation theory for the finite element analysis of laminated composite and sandwich plates. Comput Struct 2012;94–95:45–53.
[23] Natarajan S, Manickam G. Bending and vibration of functionally graded material sandwich plates using an accurate theory. Finite Elem Anal Des 2012;57:32–42.
[24] Nguyen-Xuan H, Thai HC, Nguyen-Thoi T. Isogeometric finite element analysis of composite sandwich plates using a higher order shear deformation theory. Composites: Part B 2013;55:558–74.
[25] Thai Chien H, Ferreira AJM, Carrera E, Nguyen-Xuan H. Isogeometric analysis of laminated composite and sandwich plates using a layerwise deformation theory. Compos Struct 2013;104:196–214.
[26] Grover N, Maiti DK, Singh BN. A new inverse hyperbolic shear deformation theory for static and buckling analysis of laminated composite and sandwich plates. Compos Struct 2013;95:667–75.
[27] Neves AMA, Ferreira AJM, Carrera E, Cinefra M, Roque CMC, Jorge RMN, et al. Static, free vibration and buckling analysis of isotropic and sandwich functionally graded plates using a quasi-3D higher-order shear deformation theory and a meshless technique. Compos Part B: Eng 2013;44:657–74.
[28] Fazzolari FA, Carrera E. Thermal stability of FGM sandwich plates under various through-the-thickness temperature distributions. J Therm Stress 2014;0:1–33.
[29] Fazzolari FA, Carrera E. Refined hierarchical kinematics quasi-3D Ritz models for free vibration analysis of doubly curved FGM shells and sandwich shells with FGM core. J Sound Vib 2014;333:1485–508.
[30] Fazzolari FA, Carrera E. Coupled thermoelastic effect in free vibration analysis of anisotropic multilayered plates and FGM plates by using a variable-kinematics Ritz formulation. Eur J Mech A/Solids 2014;44:157–74.
[31] Carrera E, Cinefra M, Fazzolari FA. Some results on thermal stress of layered plates and shells by using unified formulation. J Therm Stress 2013;36:589–625.
[32] Cinefra M, Carrera E, Della Croce L, Chinosi C. Refined shell elements for the analysis of functionally graded structures. Compos Struct 2012;94:415–22.
[33] Brischetto S, Carrera E. Coupled thermo-mechanical analysis of one-layered and multilayered plates. Compos Struct 2010;92:1793–812.
[34] Golmakani ME. Large deflection thermoelastic analysis of shear deformable functionally graded variable thickness rotating disk. Composites: Part B 2013;45:1143–55.
[35] Torabi J, Kiani Y, Eslami MR. Linear thermal buckling analysis of truncated hybrid FGM conical shells. Composites: Part B 2013;50:265–72.
[36] Malekzadeh P, Monajjemzadeh SM. Dynamic response of functionally graded plates in thermal environment under moving load. Composites: Part B 2013;45:1521–33.
[37] Kiani Y, Eslami MR. An exact solution for thermal buckling of annular FGM plates on an elastic medium. Composites: Part B 2013;45:101–10.
[38] Hamidi A, Zidi M, Houari MSA, Tounsi A. A new four variable refined plate theory for bending response of functionally graded sandwich plates under thermomechanical loading. Composites: Part B 2012. http://dx.doi.org/10.1016/j.compositesb.2012.03.021.
[39] Houari MSA, Tounsi A, Anwar Bég O. Thermoelastic bending analysis of functionally graded sandwich plates using a new higher order shear and normal deformation theory. Int J Mech Sci 2013;76:102–11.
[40] Tounsi A, Houari MSA, Benyoucef S, Adda Bedia EA. A refined trigonometric shear deformation theory for thermoelastic bending of functionally graded sandwich plates. Aerospace Sci Technol 2013;24:209–20.
[41] Mantari JL, Guedes Soares C. A trigonometric plate theory with 5-unknowns and stretching effect for advanced composite plates. Compos Struct 2014;107:396–405.
[42] Koiter WT. A consistent first approximation in the general theory of thin elastic shells. In: Proceedings of first symposium on the theory of thin elastic shells. Amsterdam: North-Holland; 1959.
[43] Reddy JN, Liu CF. A higher-order shear deformation theory of laminated elastic shells. Int J Eng Sci 1985;23:319–30.
[44] Touratier M. An efficient standard plate theory. Int J Eng Sci 1991;29(8):901–16.
[45] Karama M, Afaq KS, Mistou S. Mechanical behavior of laminated composite beam by the new multilayered laminated composite structures model with transverse shear stress continuity. Int J Solid Struct 2003;40(6):1525–46.
[46] Karama M, Afaq, KS, Mistou S. A new theory for laminated composite plates. In: Proc IMechE 2009, vol. 223. Part L: J Mater: Des Appl.